BIOCHEMISTRY
including biophysical chemistry & molecular biology

Article

pubs.acs.org/biochemistry

Characterization of Red/Green Cyanobacteriochrome NpR6012g4 by Solution Nuclear Magnetic Resonance Spectroscopy: A Protonated Bilin Ring System in Both Photostates

Nathan C. Rockwell,[†] Shelley S. Martin,[†] Sunghyuk Lim,[‡] J. Clark Lagarias,[†] and James B. Ames*[,‡]

[†]Department of Molecular and Cellular Biology and [‡]Department of Chemistry, University of California, Davis, California 95616, United States

Supporting Information

ABSTRACT: Cyanobacteriochromes (CBCRs) are cyanobacterial photoreceptors distantly related to phytochromes. Both CBCRs and phytochromes use photoisomerization of a linear tetrapyrrole (bilin) chromophore to photoconvert between two states with distinct spectral and biochemical properties, the dark state and the photoproduct. The isolated CBCR domain NpR6012g4 from *Nostoc punctiforme* is a well-characterized member of the canonical red/green CBCR subfamily, photosensory domains that can function as sensors for light color or intensity to regulate phototactic responses of filamentous cyanobacteria. Such red/green CBCRs utilize conserved Phe residues to tune the photoproduct for green light absorption, but conflicting interpretations of the photoproduct chromophore structure have been proposed. In the hydration model, the proposed photoproduct state is extensively solvated, with a loosely bound, conformationally flexible chromophore. In the trapped-twist model, the photoproduct chromophore is sterically constrained by hydrophobic amino acids, including the known Phe residues. Here, we have characterized chromophore structure in NpR6012g4 using solution nuclear magnetic resonance spectroscopy and a series of labeled chromophores. Four NH resonances are assigned for both the red-absorbing dark state and the green-absorbing photoproduct. Moreover, observed ^{13}C chemical shifts are in good agreement with those obtained for protonated rather than deprotonated bilins in *ab initio* calculations. Our results demonstrate that NpR6012g4 has a protonated, cationic bilin π system in both photostates, consistent with a photoproduct structure in which the chromophore is not extensively hydrated.

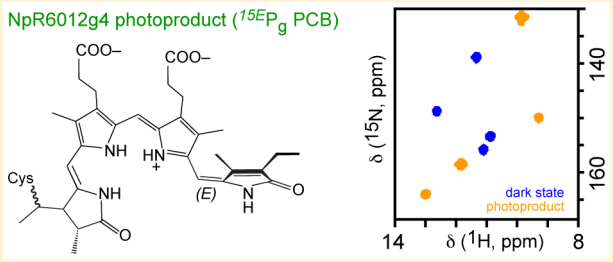

Photosynthetic organisms often optimize their light-harvesting systems in response to changes in ambient light or other metabolic challenges. As an example, most cyanobacteria use phycobilisomes for light harvesting. These large protein complexes use linear tetrapyrrole (bilin) chromophores derived from the oxidative breakdown of heme to harvest light and to transfer it to the photosynthetic reaction centers.[1,2] Iron depletion can lead to replacement of bilin-based light harvesting with alternative chlorophyll-based systems,[3−5] reducing the demand for heme under such conditions. Many cyanobacteria can change the bilin composition of the phycobilisome in response to the color of the ambient light, a process known as complementary chromatic acclimation (CCA).[6] More recently, cyanobacteria have been shown to exhibit a similar response to permit growth in far-red light.[7] This FaRLiP response involves complete restructuring of photosynthetic reaction centers, with synthesis of red-shifted Chl *d* and *f* as well as induction of red-shifted phycobiliproteins. Cyanobacteria can also use the color of ambient light to regulate the transition between motile and sessile lifestyles[8] and to exhibit both positive and negative phototaxis, moving toward photosynthetically active blue and red light and away from dangerous UV light.[9−16]

Such flexible, diverse photobiology relies on the function of an extensive array of photoreceptors interfaced with signal transduction pathways that integrate photosensory information for photobiological outputs. Cyanobacteria make extensive use of the phytochrome superfamily of photoreceptors,[6−15,17−20] which utilize covalently attached bilin chromophores similar to those of phycobiliproteins.[21−24] Canonical phytochromes reversibly photoconvert between red- and far-red-absorbing photostates (P_r and P_{fr}, respectively) via photoisomerization of the 15,16-double bond of the bilin chromophore.[22,25−27] Phytochrome photoreceptors are found in fungi, cyanobacteria, nonoxygenic photosynthetic bacteria, nonphotosynthetic bacteria, and eukaryotic algae in addition to those found in land plants that were first described more than 50 years ago.[18,28−36]

Cyanobacteria also contain cyanobacteriochromes (CBCRs), a family of photoreceptors distantly related to phytochromes.[37] Like cyanobacterial phytochromes, CBCRs use phycocyanobilin (PCB) as a chromophore precursor, with covalent linkage occurring autocatalytically between the C3[1] atom of PCB and a

Received: December 20, 2014
Revised: March 13, 2015
Published: April 6, 2015

DOI: 10.1021/bi501548t
Biochemistry 2015, 54, 2581−2600

conserved Cys residue (Figure S1 of the Supporting Information). CBCRs are frequently found as modular components in larger signaling molecules associated with a variety of signaling outputs and can occur in tandem with phytochromes or with other CBCRs.[23] CBCRs are known to regulate CCA, phototaxis, and the transition between planktonic and sessile lifestyles.[6,8−15,17,19,20] However, a single cyanobacterial genome may contain more than 20 genes containing CBCR sensors,[38] so it seems plausible that CBCRs may regulate other aspects of cyanobacterial metabolism that have not yet been recognized.

There is an ever-expanding list of recognized CBCR subfamilies.[19,37−43] CBCRs exhibit a great variety of photocycles spanning the visible spectrum and the near-ultraviolet range,[37,41,44,45] but these photocycles all exploit the same primary photoisomerization between 15*Z* and 15*E* configurations of the bilin chromophore.[37,41,46−50] For PCB, these configurations intrinsically absorb red and orange light, respectively (Figure 1A);[51] therefore, CBCR spectral diversity is generated via several tuning mechanisms. At least two CBCR lineages, the NpR3784 group and the canonical red/green CBCRs, exhibit red/green photocycles (Figure 1B).[38,39,52] The red/green photocycles of both subfamilies are very similar despite their independent evolutionary histories and their use of different residues in spectral tuning.[38,43] In such photocycles, a red-absorbing 15*Z* dark state ($^{15Z}P_r$) interconverts with a green-absorbing 15*E* photoproduct ($^{15E}P_g$). The green-absorbing photoproduct is thus blue-shifted by the CBCR relative to the intrinsic orange absorption of 15*E* PCB. Regeneration of $^{15Z}P_r$ can be driven by green light or can occur spontaneously in a process known as dark reversion. Little is yet known about dark reversion rates in the NpR3784 lineage of red/green CBCRs, but dark reversion varies over several orders of magnitude in canonical red/green CBCRs such as NpR6012g4 and NpF2164g6.[52] This wide range of dark reversion rates allows the canonical red/green CBCRs to function either as color sensors or as broadband sensors of light intensity.

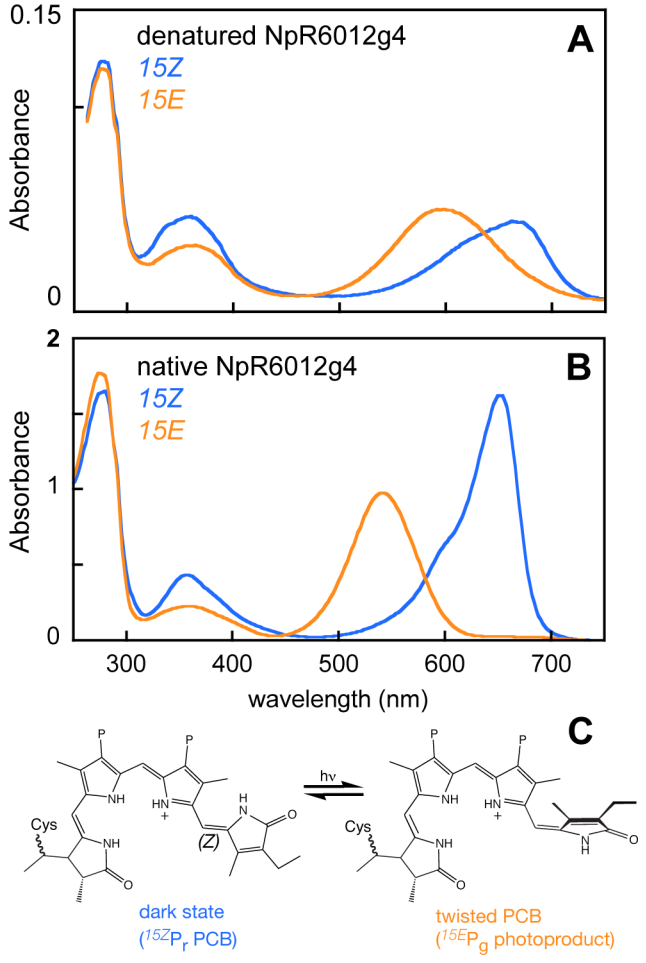

Figure 1. Red/green photocycle of NpR6012g4. (A) Absorption spectra are shown for denatured NpR6012g4 in the 15*Z* dark state (blue) and 15*E* photoproduct (orange), using acidic guanidinium chloride. (B) Absorption spectra are shown for native NpR6012g4 in the 15*Z* dark state (blue) and 15*E* photoproduct (orange). (C) Trapped-twist model for the red/green photocycle.

The crystal structure of the red-absorbing dark state of the canonical red/green CBCR AnPixJg2[49] is the only structural information available for this CBCR subfamily. The structural basis for the photoproduct blue shift of red/green CBCRs thus remains uncertain. Resonance Raman spectroscopy on AnPixJg2 provided support for a protonated, cationic bilin ring system in the photoproduct.[53] This result is not consistent with a protochromic photocycle analogous to those seen in green/red CBCRs regulating CCA (Figure S2A of the Supporting Information).[51] However, AnPixJg2 and other red/green CBCRs are known to be heterogeneous.[43,52−58] It is thus possible that this heterogeneity could confound interpretation of the vibrational spectra. A detailed analysis of the resonance Raman studies in combination with molecular dynamics simulations led to the proposal that the photoproduct of AnPixJg2 is extensively solvated because of movement of a conserved "lid" Trp residue (Figure S2B of the Supporting Information).[53] However, the lid Trp is not essential for the red/green photocycle of NpR6012g4 and is absent in NpR5113g2, which exhibits a normal red/green photocycle.[43,52] Moreover, the proposed solvation of the photoproduct by multiple water molecules able to exchange with bulk solvent is inconsistent with a protonated chromophore, given an intrinsic pK_a of 5.8 for the bilin ring system of the denatured NpR6012g4 photoproduct.[51] The original characterization of AnPixJg2[39] led to the proposal that the chromophore was trapped in a twisted configuration in the photoproduct state (Figure 1C), as is seen for the photoactive biliprotein α-phycoerythrocyanin.[59] This trapped-twist hypothesis has received recent support with the demonstration that conserved Phe residues are specifically required for photoproduct tuning in both NpR6012g4 and NpR5113g2.[43]

Thus, there are three competing models for photoproduct tuning in red/green CBCRs (Figure 1C and Figure S2 of the Supporting Information): a protochromic model, a solvation model with a flexible pocket for the bilin D-ring and a chromophore exposed to bulk solvent, and a trapped-twist model with a rigid, hydrophobic pocket for the D-ring. These models make different predictions about the protonation state and charge of the bilin π system. The protochromic model explicitly predicts a deprotonated, neutral bilin π system in the photoproduct (Figure S2A of the Supporting Information). The pK_a of the bilin-conjugated system of NpR6012g4 is ∼5.8 under denaturing conditions.[51] A solvated chromophore-binding pocket should have a similar value, because the effects of specific protein residues would be reduced in such a conformationally flexible, extensively hydrated environment. Red/green CBCRs are typically characterized at pH 7−

DOI: 10.1021/bi501548t
Biochemistry 2015, 54, 2581−2600

8.5.[38,39,43,52−57,60−62] One would thus expect formation of a deprotonated, neutral bilin π system in the photoproduct under the solvation model (Figure S2B of the Supporting Information). By contrast, the trapped-twist model postulates a rigid photoproduct pocket in which spectral tuning is determined by planar, hydrophobic Phe residues.[43] In this hydrophobic environment, the bilin ring system would be excluded from proton acceptors and hence would remain in the protonated, cationic state (Figure 1C).

Here, we characterize the red/green photocycle of the isolated CBCR domain NpR6012g4 using solution NMR spectroscopy. Our studies exploit a series of samples recombinantly expressed in *Escherichia coli* grown in the presence of isotopically labeled δ-aminolevulinic acid (ALA), the committed precursor for tetrapyrrole synthesis and hence for labeling the bilin chromophore. By varying the label in ALA, we obtained NpR6012g4 samples with distinct PCB labeling patterns (Figure S1 and Table S1 of the Supporting Information). We then used solution NMR spectroscopy to obtain complete assignments for the NpR6012g4 chromophore in both photostates that were corroborated by *ab initio* calculations. Our results clearly demonstrate a protonated chromophore ring system in both NpR6012g4 photostates, supporting the trapped-twist model for photoproduct tuning.

MATERIALS AND METHODS

Expression and Purification of NpR6012g4. NpR6012g4 was expressed using the previously described intein-chitin-binding domain construct[52,56] in BL21-AI cells (Invitrogen) grown in M9 minimal medium supplemented with ALA to a final concentration of approximately 100 μM. [5-^{13}C]ALA and [U-^{13}C,^{15}N]ALA were from Sigma. [^{15}N]ALA was from Medical Isotopes. [2-^{13}C]Indole, [^{15}N]indole, and [4-^{13}C]ALA were from Cambridge Isotope Laboratories. For some expressions, ammonium chloride labeled with ^{15}N (Cambridge) was used for the M9 medium. Frozen cell pellets were lysed in a microfluidizer, followed by ultracentrifugation and loading onto a chitin column as previously described. After the sample had bound to the chitin column and overnight incubation with dithiothreitol at 4 °C for elution, peak fractions were pooled for overnight dialysis against 10 mM sodium phosphate and 1 mM EDTA (pH 7.4) followed by overnight dialysis into 10 mM sodium phosphate (pH 7.4). NMR samples were then prepared by concentrating to a final protein concentration of approximately 0.4 mM, followed by addition of D_2O to a concentration of 7% (v/v). The level of contaminating apoprotein was very low: this procedure yielded purified protein with specific absorbance ratio (SAR) values of 1.2−1.5, in excess of the previously reported value of 0.9.[52]

Preparation of Dark-Adapted and Light-Adapted NpR6012g4. The dark-state NpR6012g4 sample for NMR experiments was prepared by illuminating a 0.5 mL sample in an NMR tube with 532 nm laser excitation at 5 mW for 5 min. The green-absorbing photoproduct was generated by illuminating the sample for 10 min with 632.8 nm laser excitation at 2 mW. The rate constant for dark reversion was estimated to be 0.08 h^{-1} at 298 K. The percentage of dark reversion during the longest NMR experiment (24 h) was <25% as judged by measuring the relative NMR intensity of a resolved upfield proton resonance at −0.4 ppm (characteristic of the photoproduct) before and after each multidimensional NMR experiment (Figure S3B of the Supporting Information, asterisk). The overall sample quality and efficiency of ALA incorporation were also confirmed by ^{1}H−^{15}N HSQC spectroscopy (Figure S3C−E of the Supporting Information).

NMR Spectroscopy. All NMR experiments were performed using a Bruker 600 MHz Avance III spectrometer equipped with a triple-resonance cryogenic TCI probe and pulsed field gradients,[63,64] with spectral acquisition at 298 K. NMR data were processed using the NMRPipe software package[65] and analyzed using SPARKY (www.cgl.ucsf.edu/home/sparky). One-dimensional (1D) ^{13}C NMR spectra (with ^{1}H decoupling by WALTZ-16 applied during the acquisition) were acquired with 2048 scans, a recycle delay of 2 s, and an acquisition time of 1.1 s to permit resolution of 0.01 ppm at a spectral sweep width of 200 ppm. The ^{13}C carrier frequency was 100 ppm.

^{1}H−^{15}N Correlation Spectroscopy. Pyrrole NH NMR resonances from ^{15}N-labeled bilin chromophore attached to unlabeled NpR6012g4 protein were detected using ^{1}H−^{15}N HSQC[66] with WATERGATE solvent suppression.[66] The NOE mixing time was 120 ms. Bilin ^{15}N correlations with adjacent ^{13}C carbonyl resonances (at C1 and C19) were detected by HNCO,[67] and bilin ^{15}N correlations with adjacent aromatic ^{13}C resonances were detected by a modified version of HNCA (dubbed HNC$_{ar}$) in which the ^{13}C carrier frequency was adjusted to 130 ppm (instead of 54 ppm used in HNCA)[67] with a ^{15}N−C$_{ar}$ rephasing time of 12.5 ms. Two-dimensional ^{15}N−^{1}H long-range HMQC (LR-HMQC) experiments used a dephasing delay of 45 ms with the GARP sequence for decoupling of ^{15}N. The sample labeled with [5-^{13}C]ALA also carried a ^{15}N label on the protein (using growth in [^{15}N]ammonium chloride). The carrier frequencies and spectral acquisition times for each experiment are indicated in the figure legends.

^{1}H−^{13}C Correlation Spectroscopy. Bilin proton resonances attached to ^{13}C were selectively detected by isotope-edited ^{1}H−^{13}C correlation NMR experiments on various ^{13}C-labeled bilin chromophores attached to unlabeled NpR6012g4 protein. The experimental parameters used for conventional ^{1}H−^{13}C correlation NMR experiments have been described previously: ^{1}H−^{13}C HMQC[68] and HMBC.[69] The NOE mixing time in all ^{13}C/^{15}N-edited NOESY-HSQC experiments was 120 ms.

***Ab Initio* Calculations.** Initial geometries were constructed in several different configurations using MacMolPlt.[70] To permit a rapid survey of different conditions, these geometries were optimized at the AM1 level in GAMESS.[71] B3LYP/6-31G* NMR deshielding calculations and BLYP/6-31G* TD-DFT calculations on the resulting geometries were performed in Gaussian03.[72] TD-DFT calculations for the protonated A-α_f D-α_f C5-*Z,syn* C10-*Z,syn* C15-*Z,anti* geometry mimicking the 15*Z* red-absorbing dark state have been described previously;[73] geometry optimization and TD-DFT calculations for deprotonated tautomers followed the published procedure. Results from ^{13}C deshielding calculations are reported relative to the calculated value for TMS.

RESULTS

Overall Assignment Strategy. We sought to examine chromophore structure in NpR6012g4 using solution NMR spectroscopy. Our strategy relied on use of the committed chromophore precursor ALA with different isotopic labeling patterns (Figure S1 and Table S1 of the Supporting Information) to generate specific chromophore labeling

DOI: 10.1021/bi501548t
Biochemistry 2015, 54, 2581−2600

patterns with good enrichment over natural abundance protein signals. To confirm efficient ALA incorporation, we compared two-dimensional (2D) $^{1}H-^{15}N$ HSQC of NpR6012g4 purified after expression in cells grown in ^{15}N-labeled medium without ALA or with [C5-^{13}C]ALA (Table S1 of the Supporting Information). The [C5-^{13}C]ALA contained natural abundance nitrogen, so its incorporation into the chromophore would suppress incorporation of the ^{15}N-labeled chromophore arising due to endogenous ALA synthesis. One-dimensional ^{1}H spectra and 2D $^{1}H-^{15}N$ HSQC spectra of the C5 sample were both consistent with a folded protein (Figure S3A–C of the Supporting Information). The suppression of bilin NH peaks in 2D $^{1}H-^{15}N$ HSQC spectra (Figure S3D,E of the Supporting Information) confirmed that this labeling scheme yielded efficient incorporation of exogenous ALA into the purified holoprotein, estimated to be ≥90% using this method. These experiments thus validated the approach, allowing us to employ different labeling patterns (Figure S1 of the Supporting Information) and pulse sequences (Figure S4 of the Supporting Information) in an overall strategy leading to complete assignment of the PCB chromophore (Figure S5 of the Supporting Information).

Partial Assignment Using Selective ^{13}C Labeling with [C5-^{13}C]ALA. Utilization of [C5-^{13}C]ALA during biosynthesis of the PCB chromophore causes incorporation of ^{13}C at C4, C5, C9–C11, C15, and C19 (Figure S1 of the Supporting Information). The one-dimensional, proton-decoupled ^{13}C NMR spectrum revealed several clear peaks for the red-absorbing dark state, along with natural abundance protein peaks having chemical shifts of <50 ppm (Figure 2A). The singlet peak detected downfield at 174 ppm was assigned to the carbonyl C19 atom based on the labeling pattern (Figure S1 of the Supporting Information), consistent with similar chemical shift values for C19 in other bilin-based photoreceptors.[25,27,74] Three peaks were detected within the expected range for bilin methines: a doublet at 89 ppm, a singlet at 95 ppm, and a triplet at 114 ppm. C5 is adjacent to labeled C4 and unlabeled C6 atoms in this labeling scheme; on the other hand, C15 is not adjacent to labeled atoms and C10 is adjacent to two labeled atoms (C9 and C11). We therefore used the C–C splitting pattern to assign C5 to 89 ppm, C10 to 114 ppm, and C15 to 95 ppm (Table 1). The remaining unassigned bilin peaks are a doublet at 148 ppm with a *J* coupling of 81 Hz and a pair of doublets at approximately 128 and 130 ppm, both having *J* coupling of 75 Hz. The *J* coupling of the peak at 148 ppm (81 Hz) matches that of C5, allowing assignment of the 148 ppm peak to C4 (Table 1). The *J* couplings (75 Hz) of the two doublets centered at 128 and 130 ppm both match the *J* splitting of C10 and therefore arise from C9 and C11.

We next assigned bilin H atoms for the red-absorbing dark state. We initially performed 2D $^{13}C-^{1}H$ HMQC experiments (Figure 3A) to detect the methine protons (Figure S4 of the Supporting Information). Despite the presence of natural abundance signals from the protein, each methine C was associated with a single cross-peak. We assigned ^{1}H chemical shifts of 5.8, 6.5, and 4.3 ppm to H5, H10, and H15, respectively (Table 1). We then used $^{13}C-^{1}H$ HMBC to resolve additional bilin H atoms two or three bonds away from the labeled C atoms (Figure S4 of the Supporting Information). Given the [C5-^{13}C]ALA labeling pattern, such H atoms are attached to C2, C3, C3^{1}, C8^{1}, C12^{1}, and C18^{1} (Figure S1 of the Supporting Information). Again, natural abundance signals predominated (Figure 4A), with only a single weak cross-peak

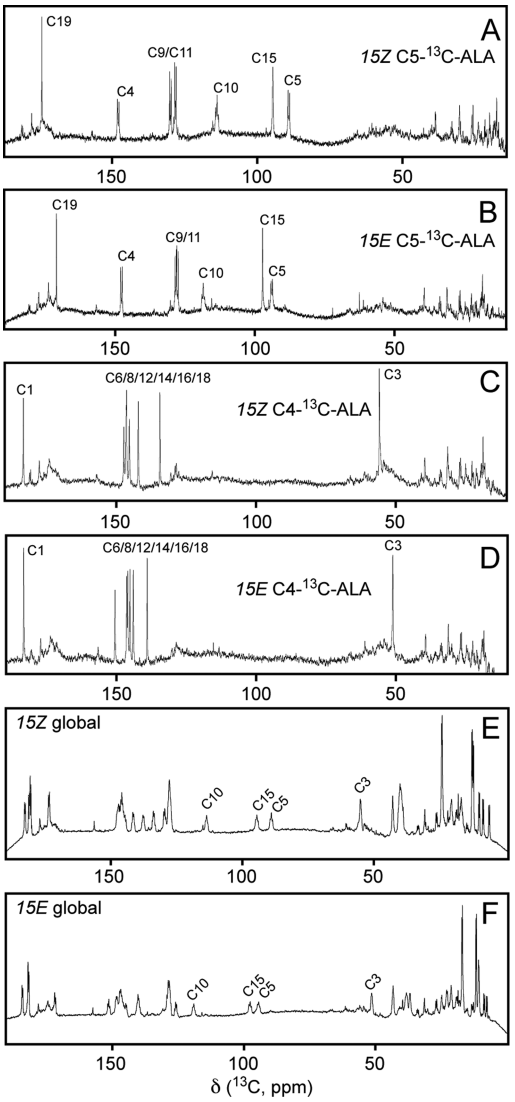

Figure 2. One-dimensional ^{13}C spectra of selectively labeled NpR6012g4. (A) NpR6012g4 labeled with [C5-^{13}C]ALA is shown in the red-absorbing 15*Z* dark state. (B) NpR6012g4 labeled with [C5-^{13}C]ALA is shown in the green-absorbing 15*E* photoproduct. (C) NpR6012g4 labeled with [C4-^{13}C]ALA is shown in the red-absorbing 15*Z* dark state. (D) NpR6012g4 labeled with [C4-^{13}C]ALA is shown in the green-absorbing 15*E* photoproduct. (E) NpR6012g4 with globally labeled chromophore is shown in the red-absorbing 15*Z* dark state. (F) NpR6012g4 with globally labeled chromophore is shown in the green-absorbing 15*E* photoproduct. The ^{13}C carrier frequency was 100 ppm, and the acquisition time was 1.1 s.

matching a known bilin chemical shift. This peak matches C4 [148 ppm (Table 1)], with the proton at approximately 3.5 ppm. This chemical shift value is consistent with a tertiary H atom, as expected for a two-bond coupling to H3 or a three-bond coupling to H2 or H3^{1}.

The 1D ^{13}C NMR spectrum of the photoproduct labeled with [C5-^{13}C]ALA again revealed clear peaks for the green-absorbing 15*E* photoproduct of NpR6012g4 (Figure 2B). Using the same logical process as for the 15*Z* dark state, we assigned peaks at 148, 94, 118.5, 97, and 171.3 ppm to C4, C5, C10, C15, and C19, respectively (Table 1). C9 and C11 were again identified as a pair of peaks at 128.5 and 129 ppm. HMQC spectroscopy allowed us to assign H5, H10, and H15 to 5.5, 7.2, and 6.2 ppm, respectively (Figure 3B). The HMBC

DOI: 10.1021/bi501548t
Biochemistry 2015, 54, 2581–2600

Table 1. ^{1}H, ^{13}C, and ^{15}N Chemical Shifts of the NpR6012g4 Chromophore[a]

position	15Z δ (^{13}C, ppm)	15Z δ (^{1}H, ppm)	15E δ (^{13}C, ppm)	15E δ (^{1}H, ppm)
C1	183.3	–	183.6	–
C2	40.5	2.6	36.4	2.6
$C2^{1}$	12.9	1.4	16.9	1.1
C3	55.9	3.5	51.1	2.7
$C3^{1}$	43.5	3.1	43	3.3
$C3^{2}$	25	1.8	10.6	0.9
C4	148	–	148	–
C5	89	5.8	94	5.5
C6	147.2	–	150.9	–
C7	128.2	–	127.5	–
$C7^{1}$	9	2.1	8.5	1.6
C8	146.5	–	146.7	–
$C8^{1}$	21.3	2.1; 2.8	22.8	1.5; 2.6
$C8^{2}$	41	2.1; 2.7	37.8	2.0; 2.2
$C8^{3}$	181.7	–	181.3	–
C9	130	–	129	–
C10	114	6.5	118.5	7.2
C11	128.3	–	128.5	–
C12	142.1	–	144.3	–
$C12^{1}$	24.6	2.8; 3.0	21.1	2.4; 3.8
$C12^{2}$	40	2.0; 2.6	38.3	2.2; 2.8
$C12^{3}$	181.2	–	181.5	–
C13	127.2	–	125.3	–
$C13^{1}$	10.4	1.84	7.5	1.2
C14	146.3	–	146.2	–
C15	95	4.3	97	6.2
C16	145.2	–	145.5	–
C17	137.9	–	139.9	–
$C17^{1}$	6.7	−0.3	11.6	1.7
C18	134.3	–	139.3	–
$C18^{1}$	17.2	a, 0.8; b, 2.05	16.6	a, 1.8; b, 2.0
$C18^{2}$	13	0.3	11.5	0.4
C19	174	–	171.3	–
position	15Z δ (^{15}N, ppm)	15Z δ (^{1}H, ppm)	15E δ (^{15}N, ppm)	15E δ (^{1}H, ppm)
NH_A	155	11.1	149.8	9.3
NH_B	148	12.7	163.9	13
NH_C	154	10.9	158.5	11.9
NH_D	138	11.35	131.5	9.9

[a]Aromatic ring carbons lack attached H atoms. Two proton resonances were observed for all methylene carbons. At $C18^{1}$, the two protons exhibited slightly different NOESY cross-peaks and are therefore designated $H18^{1}_{a}$ and $H18^{1}_{b}$.

experiment again gave a single cross-peak to C4 from a proton having a chemical shift of 2.7 ppm (Figure 4B). This value again seemed to be consistent with H3, H2, or $H3^{1}$.

Partial Assignment Using Selective ^{13}C Labeling with [C4-^{13}C]ALA. We next examined NpR6012g4 prepared after labeling with [C4-^{13}C]ALA, which labels C1, C3, C6, C8, C12, C14, C16, and C18 (Figure S1 of the Supporting Information). In this case, no two ^{13}C atoms are adjacent, so C−C splitting could not be used in the assignment process. The 1D ^{13}C spectrum of the red-absorbing dark state showed a clear singlet at 183.3 ppm and another at 55.9 ppm (Figure 2C). The downfield peak occurs in the carbonyl region and hence was assigned to C1, whereas the upfield peak at 55.9 ppm is consistent with a tertiary aliphatic carbon and was assigned to C3 (Table 1). The six remaining labeled C atoms should all fall

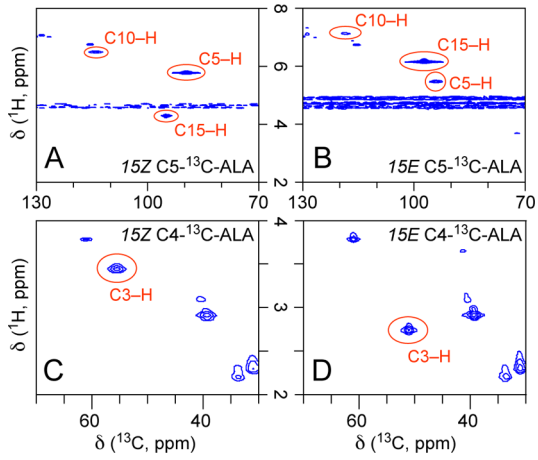

Figure 3. $^{1}H-^{13}C$ HMQC spectra of NpR6012g4 labeled with [C5-^{13}C]ALA or [C4-^{13}C]ALA. (A and B) NpR6012g4 was labeled with [C5-^{13}C]ALA. (C and D) NpR6012g4 was labeled with [C4-^{13}C]ALA. (A and C) Dark-state spectra are shown, with methine bridge cross-peaks indicated. (B and D) Photoproduct spectra are shown. The ^{13}C (F1) and ^{1}H (F2) carrier frequencies were 80 and 4.70 ppm, respectively. The acquisition times were 10.6 ms (F1) and 228 ms (F2).

in the aromatic region of the spectrum, which contained four well-resolved peaks at 134.3, 142.1, 145.3, and 147.2 ppm. There was also a pair of overlapping peaks at 146.3 and 146.5 ppm. Thus, this region of the spectrum contained the expected number of signals for this labeling pattern. The HMQC spectrum for this sample in the dark state revealed a single cross-peak to a ^{13}C chemical shift of ∼56 ppm (Figure 3C), confirming this peak as C3. The resulting value of 3.5 ppm for H3 was in agreement with the observed HMBC cross-peak from C4 in the dark state for the previous sample (Figure 4A).

The HMBC spectrum for this sample in the 15Z photostate (Figure 4A) revealed a three-bond cross-peak from C3 to 5.8 ppm, consistent with the known chemical shift of H5, and a second cross-peak from C3 to 1.4 ppm. The latter peak is not a good match for the expected chemical shift of a tertiary proton such as H2 or $H3^{1}$, but C3 could also exhibit three-bond couplings to the methyl protons at $H2^{1}$ and $H3^{2}$ (Figure S1 of the Supporting Information). There was also a cross-peak from C1 to a proton at 1.4 ppm; were this cross-peak to arise from the same proton as the cross-peak to C3, the most likely candidate would be $H2^{1}$. However, these data alone did not permit unambiguous assignment of this resonance, because these cross-peaks could also arise from separate C1−C2−$C2^{1}$−$H2^{1}$ and C3−$C3^{1}$−$C3^{2}$−$H3^{2}$ resonances with similar chemical shifts for $H2^{1}$ and $H3^{2}$. The HMBC spectrum also contained several cross-peaks from the labeled aromatic carbons to protons with chemical shift values in the range of 0−2.5 ppm, providing information about linkages between aromatic ring carbons and side-chain atoms (see below).

The 1D ^{13}C spectrum of the [C4-^{13}C]ALA sample in the photoproduct state (Figure 2D) again exhibited a carbonyl peak (183.6 ppm, C1) and a tertiary aliphatic peak (51.1 ppm, C3). Moreover, in this photostate, the aromatic region contained six cleanly resolved singlet peaks at 139.3, 144.3, 145.6, 146.3, 147.0, and 151.0 ppm, consistent with the set of C6, C8, C12, C14, C16, and C18 (Figure S1 of the Supporting Information). The HMQC spectrum gave a clear C3−H3 cross-peak (Figure 3D), yielding a chemical shift of 2.7 ppm for H3. This value is

DOI: 10.1021/bi501548t
Biochemistry 2015, 54, 2581−2600

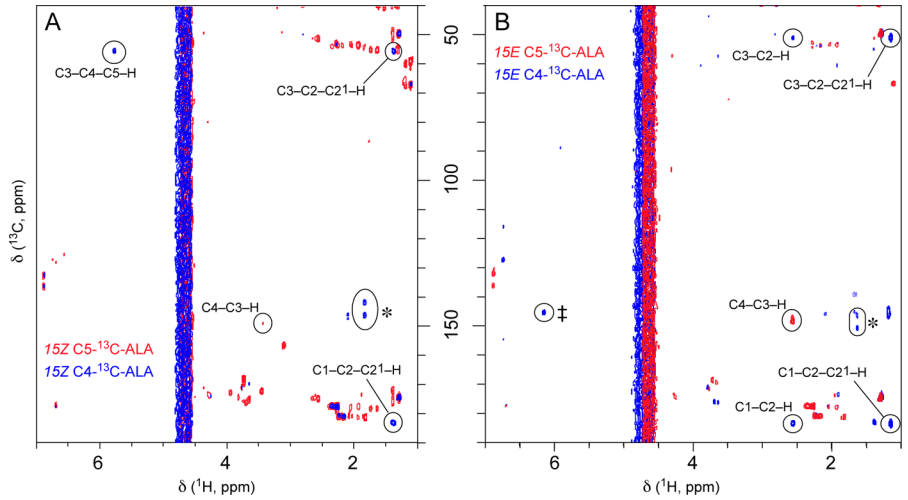

Figure 4. $^{1}H-^{13}C$ HMBC spectra of NpR6012g4 labeled with [C4-^{13}C]ALA (blue) or [C5-^{13}C]ALA (red). (A) Dark-state spectra are shown for NpR6012g4 labeled with [C5-^{13}C]ALA (red) and [C4-^{13}C]ALA (blue). (B) Photoproduct spectra are shown in the same color scheme. Asterisks indicate cross-peaks between known aromatic bilin C atoms and aliphatic H atoms. A cross-peak between an aromatic C atom and a methine H was also observed (double dagger). The ^{13}C (F1) and ^{1}H (F2) carrier frequencies were 120 and 4.70 ppm, respectively. The acquisition times were 10.6 ms (F1) and 228 ms (F2).

in good agreement with the proton observed to correlate with C4 in the 15*E* HMBC spectrum of the [C5-^{13}C]ALA sample (Figure 4B). We did not observe a C3−C4−C5−H5 cross-peak in the 15*E* HMBC spectrum for the [C4-^{13}C]ALA sample (Figure 4B). However, both C1 and C3 showed cross-peaks to a proton at 2.6 ppm and another at 1.1 ppm, implicating a chemical shift of 2.6 ppm for the tertiary H2 and a chemical shift of 1.1 ppm for H2^{1}. We again observed multiple cross-peaks in the aromatic region, including a single apparent cross-peak to H15 at approximately 145 ppm. Taken together, these experiments give chemical shift assignments for C1, C3−C5, C10, C15, and C19, along with a pair of values for C9 and C11 and a set for C6, C8, C12, C14, C16, and C18.

NpR6012g4 Contains Four Bilin NH Moieties in Both Photostates. We next characterized a sample in which bilin was labeled with [^{15}N]ALA (Figure S1 of the Supporting Information). In this experiment, Trp residues in NpR6012g4 were selectively labeled at the Cδ1 position via addition of [2-^{13}C]indole (Cambridge Isotopes) to the M9 expression medium (Table S1 of the Supporting Information).[75] Although Trp signals were detected in $^{1}H-^{13}C$ HMQC spectra (Figure S6A,B of the Supporting Information), these signals were not well-resolved and will be the subject of a future communication. The $^{1}H-^{15}N$ HSQC spectrum for the red-absorbing dark state revealed four clear N−H cross-peaks (Figure 5A), consistent with a protonated bilin ring system (Figure 1A) and with previous NMR studies of the phytochrome P_r state.[25,76] Each bilin nitrogen atom is three bonds away from a methine proton, a situation equivalent to Nδ1 and Hε1 in His residues. We therefore used long-range HMQC (LR-HMQC) to correlate bilin N atoms to the known methine H atoms (Figure S4 of the Supporting Information). The dark-state LR-HQMC spectrum (Figure 5B) showed a pair of cross-peaks to H5. The simplest interpretation of this observation would be to assign N_A and N_B as the pair of ^{15}N chemical shifts at 148.2 and 155.5 ppm, respectively, implying assignment of H_A and H_B as the pair of ^{1}H chemical shifts at 12.7 and 11.1 ppm, respectively. The other two resonances would therefore be assigned to NH_C and NH_D. However, NpR6012g4 is known to be heterogeneous,[52,54,56,57] so it was also possible that these LR-HMQC

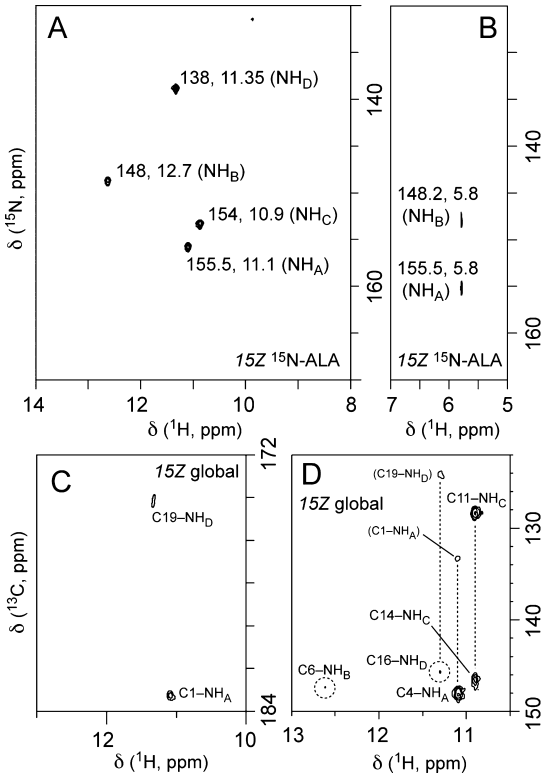

Figure 5. Characterization of bilin NH moieties in the red-absorbing NpR6012g4 dark state. (A) $^{1}H-^{15}N$ HSQC spectrum of NpR6012g4 labeled with [^{15}N]ALA. (B) $^{1}H-^{15}N$ LR-HMQC spectrum of the same sample. (C) HNCO spectrum of the ^{13}C and ^{15}N globally labeled chromophore sample. (D) HNC_{ar} spectrum of the same sample. Folded peaks are indicated in parentheses. For both HSQC and LR-HMQC, ^{15}N (F1) and ^{1}H (F2) carrier frequencies were 140 and 4.70 ppm, respectively. The acquisition times were 14 ms (F1) and 200 ms (F2). For HNCO and HNC_{ar}, ^{15}N, ^{13}C (F1), and ^{1}H (F2) carrier frequencies were 140, 130 (176 for HNCO), and 4.70 ppm, respectively. Two-dimensional acquisition times were 20 ms (F1) and 200 ms (F2).

DOI: 10.1021/bi501548t
Biochemistry 2015, 54, 2581−2600

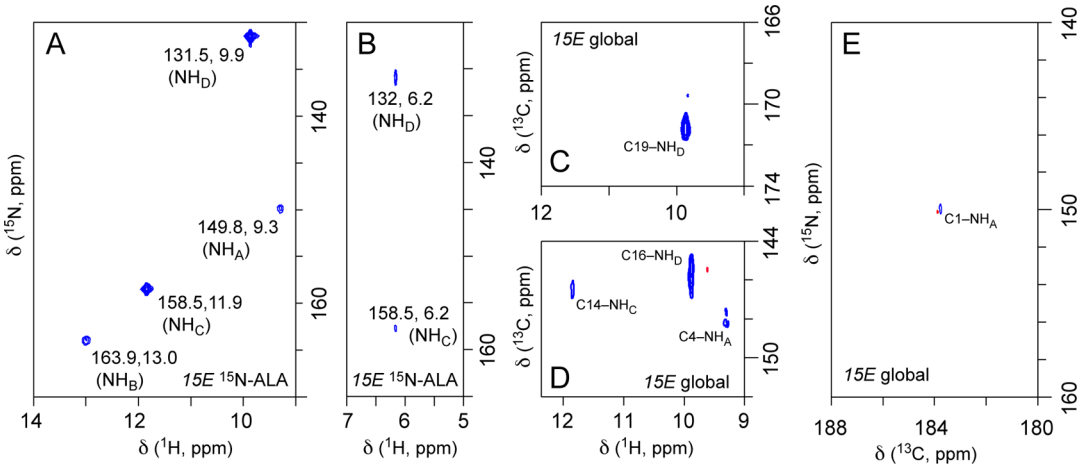

Figure 6. Characterization of bilin NH moieties in the green-absorbing NpR6012g4 photoproduct. (A) $^{1}H-^{15}N$ HSQC spectrum of the [^{15}N]ALA sample. (B) $^{1}H-^{15}N$ LR-HMQC spectrum of the same sample. (C) HNCO spectrum of the globally labeled sample. (D) HNC_{ar} spectrum of the same sample. (E) CON spectrum of the same sample. For both HSQC and LR-HMQC, ^{15}N (F1) and ^{1}H (F2) carrier frequencies were 140 and 4.70 ppm, respectively. The acquisition times were 14 ms (F1) and 200 ms (F2). For HNCO and HNC_{ar}, ^{15}N, ^{13}C (F1), and ^{1}H (F2) carrier frequencies were 140, 130 (176 for HNCO), and 4.70 ppm, respectively. Two-dimensional acquisition times were 20 ms (F1) and 200 ms (F2). The ^{15}N (F1) and ^{13}C (F2) carrier frequencies were 140 and 176 ppm, respectively. The two-dimensional acquisition times were 25 ms (F1) and 500 ms (F2). Two-dimensional spectra were acquired with 128 scans and recycle delay of 1.5 s.

resonances instead represented two chemical shifts for a single NH moiety.

To resolve this ambiguity, we noted that the A- and D-ring NH moieties are adjacent to carbonyls (Figure 1A) and hence should be accessible to pulse sequences such as HNCO[67] were the bilin to be labeled on both ^{13}C and ^{15}N (Figure S4 of the Supporting Information). Partially labeled samples had already provided information about all carbons adjacent to the NH moieties (Figure S1 of the Supporting Information), thereby permitting assignment of NH moieties prior to complete assignment of PCB C atoms. We therefore prepared an NpR6012g4 sample with global labeling of chromophore ^{13}C and ^{15}N atoms, along with labeling of all Trp side chains with ^{15}N (Table S1 of the Supporting Information). One-dimensional ^{13}C spectra of this sample (Figure 2E,F) revealed both the expected resonances and additional ones. Signals from Trp Nε1 atoms were again congested (Figure S6C,D of the Supporting Information). In the HNCO spectrum of this sample (Figure 5C), we observed a cross-peak between a ^{13}C atom at 174.2 ppm [C19 (Table 1)] and an NH proton at 11.33 ppm, identifying the NH resonance at 138/11.35 ppm as NH_D. We also observed a cross-peak between a ^{13}C atom at 183.4 ppm [C1 (Table 1)] and an NH proton at 11.1 ppm, identifying the NH resonance at 155.5/11.1 ppm as NH_A. No cross-peak was observed between C1 and the NH proton at 12.7 ppm, consistent with the possible assignment of NH_B to 148/12.7 ppm based on LR-HMQC.

We next performed an HNC_{ar} experiment (Figure S4 of the Supporting Information) to observe correlations between NH protons and adjacent aromatic carbons at C4, C6, C9, C11, C14, and C16 (Figure S1 of the Supporting Information). In this experiment, we observed two cross-peaks for three of the four NH protons detected in the $^{1}H-^{15}N$ HSQC spectrum of the red-absorbing dark state (Figure 5D). H_A (11.1 ppm) showed an aliased cross-peak to C1 and a cross-peak to C4, validating the experiment. H_D (11.35 ppm) showed an aliased cross-peak to C19 and an additional cross-peak at 145.2 ppm, matching one of the aromatic resonances observed upon labeling with [C4-^{13}C]ALA (see above). We therefore assigned this resonance to C16 (Table 1). The upfield NH proton (10.9 ppm) showed cross-peaks to 146.3 and 128.3 ppm. The cross-peak at 146.3 ppm matched an aromatic resonance observed upon labeling with [C4-^{13}C]ALA and not yet assigned (C6, C8, C12, C14, or C18). That at 128.3 ppm matches an aromatic resonance observed upon labeling with [C5-^{13}C]ALA and not yet assigned (C9 or C11). These cross-peaks could therefore arise from the B-ring (C6 and C9, adjacent to NH_B) or from the C-ring (C11 and C14, adjacent to NH_C). However, the NH proton at 10.9 ppm lacked a cross-peak to H5 in the LR-HMQC spectrum (Figure 5B), whereas the fourth resonance observed in the $^{1}H-^{15}N$ HSQC spectrum (12.7 ppm, furthest downfield) did show a cross-peak to H5. The NH proton at 12.7 ppm also exhibited a weak $^{1}H-^{13}C$ cross-peak at 147.2 ppm in the HNC_{ar} spectrum (Figure 5D), a resonance observed in the [C4-^{13}C]ALA sample. This cross-peak cannot be assigned as an alternate population of NH_A, because NH_A is adjacent to a single aromatic carbon that is labeled by [C5-^{13}C]ALA rather than by [C4-^{13}C]ALA (Figure S1 of the Supporting Information). A $^{1}H-^{13}C$ cross-peak at 147.2 ppm was not seen in the [C5-^{13}C]ALA sample (see above), which has labeled C4 and C9 atoms. Therefore, this cross-peak correlates NH_B (12.7 ppm) to C6 (147.2 ppm), and the upfield cross-peaks at 10.9 ppm correlate C11 (128.3 ppm) and C14 (146.3 ppm) to NH_C (10.9 ppm). These analyses thus resolved all four bilin NH moieties for the dark state and allowed assignment of C6, C11, C14, and C16 (Table 1).

The photoproduct $^{1}H-^{15}N$ HSQC spectrum also exhibited four N–H cross-peaks (Figure 6A), with peaks at 131.5/9.9 and 158.5/11.9 ppm being notably more intense than those at 149.8/9.3 and 163.9/13.0 ppm. The LR-HMQC spectrum of the photoproduct state again contained only two cross-peaks, in this case to H15 (Figure 6B). This observation implicates the two strong HSQC cross-peaks as NH_C and NH_D and the weaker peaks as NH_A and NH_B. However, the known heterogeneity of the photoproduct state[55,57] again implies alternate interpretations. The photoproduct HNCO spectrum for the globally labeled sample revealed a clear cross-peak between C19 and the NH_D proton (Figure 6C), assigning NH_D

DOI: 10.1021/bi501548t
Biochemistry 2015, 54, 2581–2600

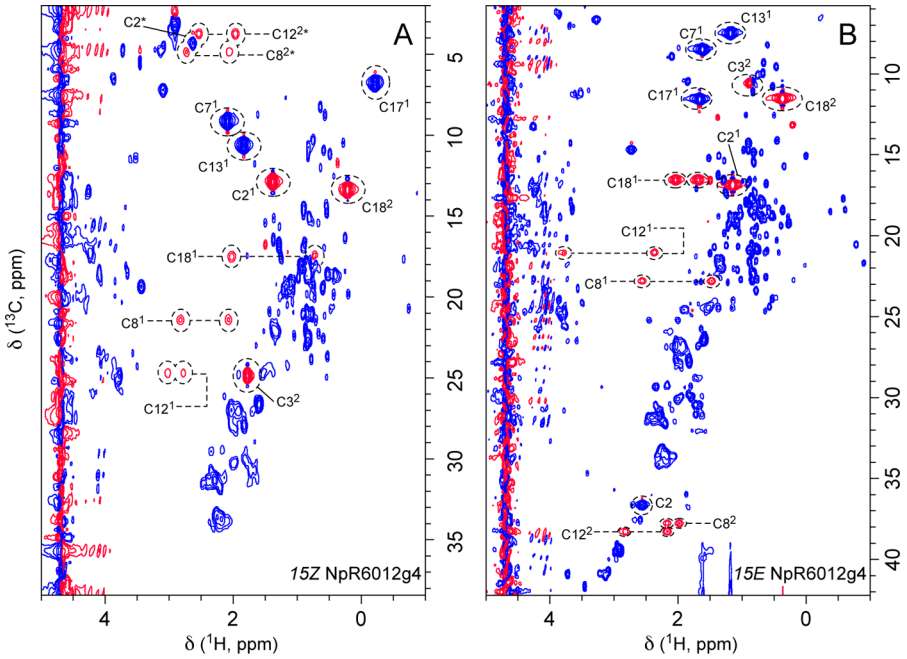

Figure 7. $^{1}H-^{13}C$ constant-time HSQC spectra of NpR6012g4. Spectra are shown for the dark state (A) and photoproduct (B), colored by phase (blue, negative; red, positive). Nonequivalent methylene protons exhibited low signal-to-noise ratios, resulting in detection of natural abundance protein resonances as well. Folded or aliased peaks are denoted with asterisks. The ^{13}C (F1) and ^{1}H (F2) carrier frequencies were 24 and 4.70 ppm, respectively. The constant-time evolution period was 13.3 ms. The two-dimensional acquisition times were 48 ms (F1) and 228 ms (F2).

to 131.5/9.9 ppm (Table 1). An HNC_{ar} experiment on this sample (Figure 6D) revealed a robust aromatic cross-peak (145.5 ppm) to the NH_D proton that matched a resonance observed in the [C4-^{13}C]ALA sample (145.6 ppm), permitting assignment of C16 (Table 1). The strong $^{1}H-^{15}N$ HSQC signal implicated as the NH_C proton by LR-HMQC exhibited a single cross-peak to a ^{13}C resonance at 146.2 ppm in HNC_{ar} (Figure 6D), again matching a ^{13}C resonance observed in the [C4-^{13}C]ALA sample (146.3 ppm). Unlike the NH_D proton, this NH proton did not exhibit a folded cross-peak to C19, consistent with assignment of NH_C to 158.5/11.9 ppm and allowing assignment of C14 (Table 1). A third, much weaker cross-peak observed in HNC_{ar} matched the known chemical shift of C4 (Figure 6D), providing a provisional assignment for NH_A (149.8/9.3 ppm). This assignment was confirmed by a two-dimensional carbon-detected CON spectrum (Figure S4 of the Supporting Information) that revealed a single $^{15}N-^{13}C$ cross-peak at the expected position for N_A-C1 (Figure 6E). Therefore, we were able to observe three of the four NH moieties in HNCO and HNC_{ar} experiments. The fourth NH moiety was observed only in the photoproduct $^{1}H-^{15}N$ HSQC spectrum (Figure 6A), in which the intensity of this resonance was comparable to that of the NH_A cross-peak. The simplest interpretation of these results is that the chromophore is protonated in both photostates, consistent with resonance Raman studies of AnPixJg2.[53] We thus assigned the fourth HSQC cross-peak to NH_B (163.9/13.0 ppm) rather than to a second population of one of the other three NH moieties (Table 1). Further support for this interpretation was obtained by complete assignment of the chromophore ^{13}C atoms and comparison of the results with *ab initio* calculations (see Discussion).

Complete Chromophore Assignments for the NpR6012g4 Dark State. We next undertook experiments to complete C and H assignments for the bilin chromophore using the strategy shown in Figure S5 of the Supporting Information. We began with detailed analysis of the ^{1}H-decoupled ^{13}C NMR spectrum of the globally labeled sample in the red-absorbing dark state (Figure S7A–C of the Supporting Information). In the carbonyl region (Figure S7A of the Supporting Information), the previously assigned C1 and C19 carbonyls now appear as doublets due to C–C splitting from the adjacent C2 and C18 atoms (Figure S1 of the Supporting Information). Two additional doublets are seen at 181–182 ppm. These are assigned to the carbonyl carbons from the propionate side chains. In the aromatic region (Figure S7B of the Supporting Information), overlapping signals occur at 125–130 and 145–150 ppm, along with multiplets at 134 and 142 ppm. Resonances at 134 and 142 ppm were previously observed in the [C4-^{13}C]ALA sample and were not assigned to C6, C14, or C16 (see above), implicating these resonances as part of an unresolved set of C8, C12, and C18. A peak at 138 ppm, not observed in previous samples (Figure S7B of the Supporting Information), must therefore correspond to the previously unlabeled C7, C13, and/or C17 atoms. The aliphatic region (Figure S7C of the Supporting Information) is more congested, with natural abundance signals from the protein along with signals from the bilin A-ring and the various side chains (Figure S1 of the Supporting Information). Notably, we observed three well-resolved doublets upfield, at 6–11 ppm (Figure S7C of the Supporting Information, asterisk). These resonances were critical in linking aliphatic side chains to aromatic ring carbons (see below).

We next examined $^{1}H-^{13}C$ HMQC and constant-time $^{1}H-^{13}C$ HSQC (ct-HSQC) spectra of the globally labeled sample in the dark state (Figure S4 of the Supporting Information). Comparison of the HMQC spectrum with those of C5-^{13}C and C4-^{13}C samples (Figure 3C,D) permitted identification of candidate C–H cross-peaks for some of the aliphatic C atoms detected in the 1D spectrum (Figure S8A of

DOI: 10.1021/bi501548t
Biochemistry 2015, 54, 2581–2600

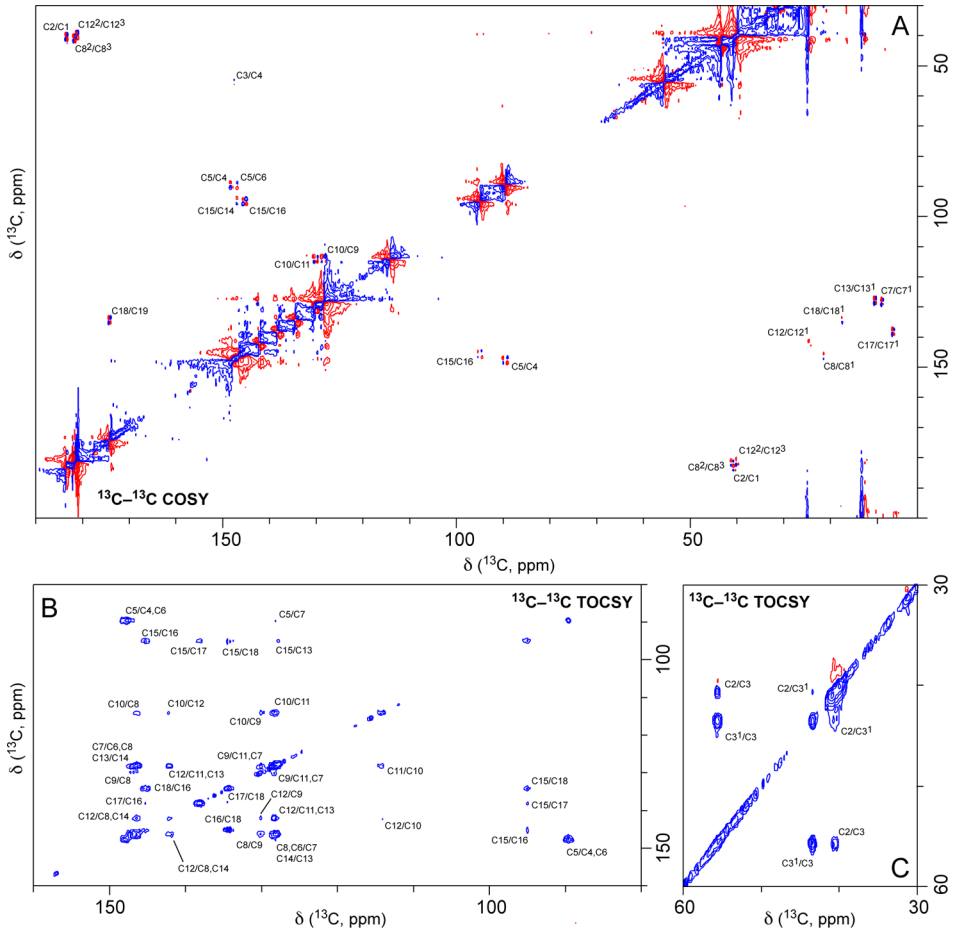

Figure 8. ^{13}C–^{13}C COSY and ^{13}C–^{13}C TOCSY spectra of the red-absorbing NpR6012g4 dark state. (A) ^{13}C–^{13}C COSY spectrum, with peak assignments indicated. No diagonal quantum filter was used to increase sensitivity, resulting in phased quadruplet peaks. Detailed views of carbonyl–aliphatic and aromatic–aliphatic cross-peaks are presented in Figure S9A,B of the Supporting Information. The ^{13}C (F1 and F2) and ^{1}H carrier frequencies were 100 and 4.70 ppm, respectively. The two-dimensional acquisition times were 10 ms (F1) and 200 ms (F2). (B) Aromatic region of the ^{13}C–^{13}C TOCSY spectrum, with peak assignments indicated. Detailed views are shown in Figure S9 of the Supporting Information. (C) Region of the ^{13}C–^{13}C TOCSY spectrum matching tertiary carbons, with peak assignments indicated. The ^{13}C TOCSY spin-locking time was 15 ms. The ^{13}C (F1 and F2) and ^{1}H carrier frequencies were 100 and 4.70 ppm, respectively. The two-dimensional acquisition times were 10 ms (F1) and 200 ms (F2). Both ^{13}C–^{13}C COSY and ^{13}C–^{13}C TOCSY spectra were acquired with 128 scans and a recycle delay of 1.5 s.

the Supporting Information). However, congestion and natural abundance signals precluded assignments based on this spectrum. The ct-HSQC spectrum proved to be more informative (Figure 7A). The three upfield C atoms identified in the 1D spectrum (Figure S7C of the Supporting Information) matched robust negative peaks at 6.7, 9.0, and 10.4 ppm. These peaks thus were good candidates for the C7^1, C13^1, or C17^1 methyl groups, because methyl ^{13}C atoms attached to aromatic ^{13}C atoms give rise to negative ct-HSQC peaks. Three robust positive peaks were also observed in the dark-state ct-HSQC spectrum. These peaks were good candidates for the C2^1, C3^2, and C18^2 methyl groups, because methyl carbons attached to aliphatic ^{13}C atoms give rise to positive ct-HSQC peaks. At several other ^{13}C chemical shifts, we also detected much weaker pairs of cross-peaks; these peaks were assigned to nonequivalent methylene protons in the propionate and 18-Et side chains (see below).

We next employed carbon-detected methods to assign all bilin ring carbon atoms, as these atoms do not have attached H atoms. A ^{13}C–^{13}C COSY spectrum (Figure 8A) revealed both several expected cross-peaks (C3–C4, C4–C5, etc.) and others that permitted additional assignments. We observed three cross-peaks between carbonyl and aliphatic carbons (Figure S9A of the Supporting Information). One of these matched the known chemical shift of C1 (Table 1), permitting assignment of C2 to 40.5 ppm. The other two were partially overlapped and matched the chemical shifts of the propionate carbonyl carbons at 181–182 ppm (Figure S7A of the Supporting Information), yielding chemical shifts for a C8^2/C12^2 pair. We also observed a cross-peak between C19 (174 ppm) and an aromatic carbon at 134.3 ppm (Figure 8A), matching a previously unassigned member of the set of C8, C12, and C18 (134.3 ppm) and hence permitting assignment of C18 (Table 1). The C7^1, C13^1, and C17^1 methyl groups each exhibited a cross-peak to an aromatic carbon (Figure S9B of the Supporting Information), implicating a set of C7, C13, and C17 of ^{13}C chemical shifts. We also observed additional cross-peaks between aromatic and aliphatic carbons (Figure S9B of the Supporting Information). One of these matched C18, permitting assignment of C18^1 [17.2 ppm (Table 1)]. The ct-HSQC spectrum for dark-state NpR6012g4 (Figure 7A) exhibited two weak cross-peaks to C18^1 at 0.8 and 2.0 ppm with the expected phase, permitting assignment of two nonequivalent H18^1 protons (Table 1). The other two COSY

DOI: 10.1021/bi501548t
Biochemistry 2015, 54, 2581–2600

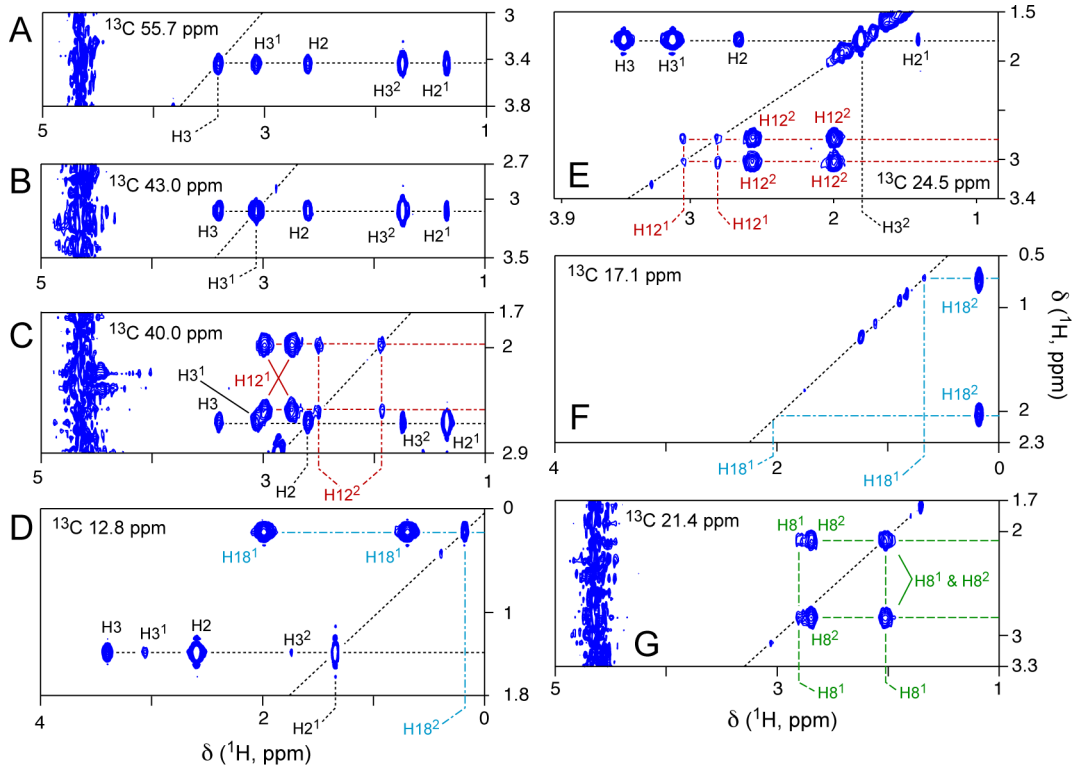

Figure 9. Mapping aliphatic resonances in the red-absorbing NpR6012g4 dark state using HCCH-TOCSY. (A–E) Strips matching aliphatic A-ring protons are shown. The slices at ^{13}C chemical shifts of 40 and 24.5 ppm, matching C2 and C3^2, respectively, also contain strips arising from the 12-propionate side chain (C and E). The slice at 12.8 ppm (D) matches C2^1 and C18^2, so a strip from H18^2 is visible. (F) Reciprocal strips from the H18^1 protons. (G) Strips for the 8-propionate. The ^{13}C (F2) and ^{1}H (F1 and F3) carrier frequencies were 40 and 4.70 ppm, respectively. The three-dimensional acquisition times were 25 ms (F1), 10 ms (F2), and 200 ms (F3).

cross-peaks in this region matched C8 and C12, permitting assignment of a C8^1/C12^1 pair. Possible cross-peaks between aliphatic carbons were present, but these were close to the diagonal and hence were not well resolved. At this point, the remaining unresolved ring carbons were the pair of C8 and C12 and the set of C7, C13, and C17.

We further characterized the dark state using ^{13}C–^{13}C TOCSY (Figure 8B,C). The aromatic region of the TOCSY spectrum contained many expected resonances and also contained potentially ambiguous, overlapped resonances (Figure 8B). Two members of the set of C7, C13, and C17 exhibited chemical shifts close to that of C11. C14 and C16 were close to each other and to one member of the pair of C8 and C12. To progress further, it was thus necessary to locate TOCSY cross-peaks that would be unambiguous. One member of the set of C7, C13, and C17 exhibited cross-peaks to C16 and C18 (Figure S9C of the Supporting Information), permitting assignment of C17 and C17^1 (Table 1). Weak cross-peaks were also observed between the methine C5 and C15 atoms and the other members of the set of C7, C13, and C17 (Figure S9D of the Supporting Information), permitting assignment of C7, C7^1, C13, and C13^1 (Table 1). The ct-HSQC spectrum then permitted assignment of H7^1, H13^1, and H17^1 (Figure 7A and Table 1). C8 and C12 remained to be assigned, and the observed TOCSY cross-peaks from these carbons were ambiguous because of the similar chemical shifts of C7, C11, and C13 (Table 1). However, the HMBC spectrum of the [C4-^{13}C]ALA sample in the 15*Z* dark state contained several cross-peaks in the aromatic region (Figure 4A, asterisk). Importantly, one of those cross-peaks could now be assigned as a three-bond correlation from C14 to the H13^1 methyl protons [C14–C13–C13^1–H13^1 (Figure S9E of the Supporting Information)]. A second HMBC cross-peak to the same proton permitted assignment of C12 at 142.1 ppm, implying the assignment of C8 at 146.5 ppm (Table 1). Consistent with this, the C12–C9 cross-peak in the TOCSY spectrum was notably weaker than the C8–C9 cross-peak and C12–C11/C13 cross-peaks (Figure S9F of the Supporting Information).

Despite having been acquired with a spin-lock pulse set to 100 ppm for resonance with the bilin π system, the ^{13}C–^{13}C TOCSY spectrum also contained signals from the aliphatic tertiary carbons of the A-ring (Figure 8C). Cross-peaks were observed between C3 and C2 (55.9 and 40.5 ppm, respectively) as well as between C3 and another C atom having a chemical shift of 43.5 ppm, which is assigned to C3^1. The carbon-detected COSY and TOCSY spectra thus permit a "walk" around the bilin ring system, despite the spectral overlap of several carbons. Starting with the known C1, the COSY spectrum reveals a cross-peak to C2. The TOCSY spectrum contains cross-peaks from C2 to C3 and from C3 to C3^1, whereas the COSY spectrum contains a cross-peak from C3 to C4. Strong cross-peaks from C4 to C5 and from C5 to C6 are seen in both spectra, and the TOCSY spectrum contains overlapping cross-peaks from C6 to C7 and from C7 to C8 as well as a well-resolved cross-peak from C8 to C9. The COSY spectrum also connects C7 to C7^1 and C8 to C8^1, and the TOCSY spectrum connects C9 to C10, C10 to C11, C11 to C12, and C12 to C13. The COSY spectrum has cross-peaks from C12 to C12^1 and C13 to C13^1, and the TOCSY C13–C14 cross-peak is overlapped with the C7–C8 cross-peak.

DOI: 10.1021/bi501548t
Biochemistry 2015, 54, 2581–2600

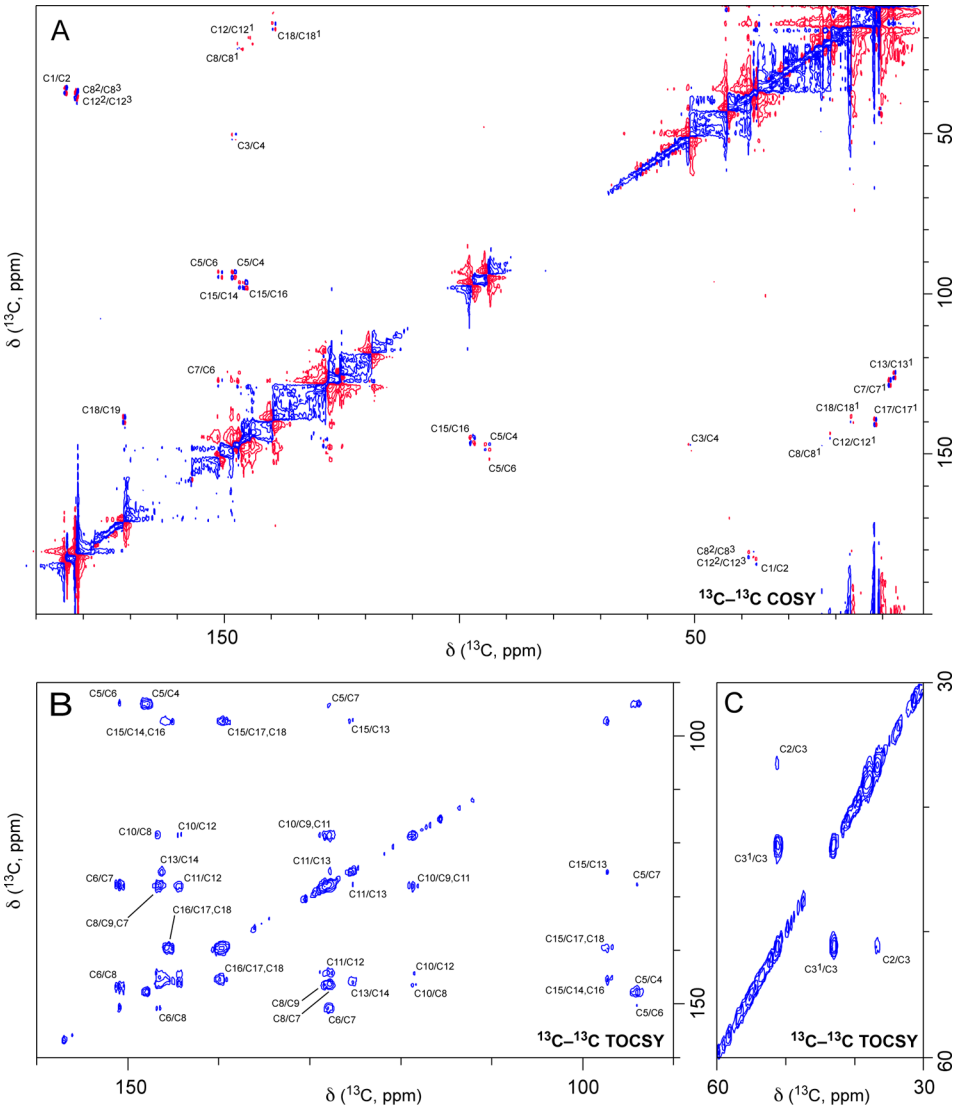

Figure 10. $^{13}C-^{13}C$ COSY and $^{13}C-^{13}C$ TOCSY spectra of the green-absorbing NpR6012g4 photoproduct. (A) $^{13}C-^{13}C$ COSY spectrum, with peak assignments indicated. No diagonal quantum filter was used to increase sensitivity. Detailed views of carbonyl−aliphatic and aromatic−aliphatic cross-peaks are presented in Figure S11 of the Supporting Information. (B) Aromatic region of the $^{13}C-^{13}C$ TOCSY spectrum, with peak assignments indicated. Detailed views are shown in Figure S11 of the Supporting Information. (C) Region of the $^{13}C-^{13}C$ TOCSY spectrum matching tertiary carbons, with peak assignments indicated. Spectral parameters were identical to those of Figure 8.

C14−C15 and C15−C16 cross-peaks can be seen in both spectra, and the TOCSY spectrum also connects C16 to C17 and C17 to C18. The COSY spectrum contains C17−C17^1, C18−C18^1, and C18−C19 cross-peaks, confirming assignment of the ring system (Figure S5 of the Supporting Information).

Remaining carbons to be assigned were thus the A-ring methyl groups at C2^1 and C3^2, the C18^2 methyl group, and the propionate side chains. Good candidates for two of the three methyl groups had already been identified by ct-HSQC (Figure 7A), and the known chemical shift of C3^1 derived from the $^{13}C-^{13}C$ TOCSY experiment permitted identification of a candidate C−H cross-peak for this atom in the $^1H-^{13}C$ HMQC spectrum (Figure S8A of the Supporting Information). For the propionates, $^{13}C-^{13}C$ COSY spectroscopy had identified C8, C8^1, C12, and C12^1 (Figure 8A). The same spectrum also contained two cross-peaks from propionate carbonyl C atoms to β-methylene groups, and the ct-HSQC spectrum provided chemical shifts for the attached protons (Figure 7A). However, we had no information to connect C8^1 to C8^2 or C12^1 to C12^2 (Figure S10 of the Supporting Information). It was thus possible that we were detecting two configurations for a single propionate side chain rather than the expected pair of side chains, in keeping with the known photochemical heterogeneity of NpR6012g4.[52,54−57]

We therefore acquired three-dimensional HCCH-TOCSY spectra (Figure 9 and Figure S4 of the Supporting Information). This experiment readily permitted assignment of the remaining A-ring resonances. The slice corresponding to C3 exhibited the expected diagonal peak at 3.45 ppm (Figure 9A) and four robust cross-peaks at 3.1, 2.6, 1.8, and 1.4 ppm. The cross-peak at 2.6 ppm is in agreement with the known chemical shift of H2, and that at 3.1 ppm matched the candidate assignment for H3^1 derived from $^{13}C-^{13}C$ TOCSY and $^1H-^{13}C$ HMQC data (Figure S8 of the Supporting Information and Table 1). By reference to the ct-HSQC spectrum, this gave values of 12.9/1.4 and 25/1.8 ppm for the 2^1 and 3^2 methyl groups (Table 1), consistent with C1−H2^1 and C3−H2^1 HMBC cross-peaks seen in the [C4-^{13}C]ALA

DOI: 10.1021/bi501548t
Biochemistry 2015, 54, 2581−2600

sample (Figure 4A). Slices matching C2 and C3^1 (Figure 9B,C) each gave both the expected diagonal peak and four robust cross-peaks matching the expected resonances. Slices matching C3^2 and C2^1 (Figure 9D,E) again exhibited the expected pattern, but resonances between H3^2 and H2^1 protons were notably weaker than other cross-peaks. A-Ring assignments were thus complete (Table 1).

HCCH-TOCSY data also permitted assignment of the 18-ethyl side chain. ^{13}C−^{13}C COSY spectroscopy provided assignment of C18^1, allowing assignment of nonequivalent H18^1 methylene protons in the ct-HSQC spectrum at 17.2/0.8 and 17.2/2.05 ppm (Figure 7A and Table 1). The ct-HSQC spectrum and assignment of the A-ring also implicated C18^2/H18^2 as the cross-peak at 13/0.3 ppm (Figure 7A). HCCH-TOCSY slices corresponding to C18^1 and C18^2 completely corroborated these assignments: the slice matching C18^1 exhibited two cross-peaks from protons at 0.8 and 2.1 ppm to a single proton at 0.3 ppm, and the slice matching C18^2 exhibited two cross-peaks from a single proton at 0.3 ppm to protons at 0.8 and 2.1 ppm (Figure 9D,F).

The ^{13}C−^{13}C COSY experiment had provided cross-peaks between C8 and C8^1, C12 and C12^1, and between the β-methylene and γ-carbonyl atoms of the two propionate side chains (Figure 8A and Figure S10 of the Supporting Information). The ct-HSQC experiment provided assignments for nonequivalent H8^1 and H12^1 protons (Table 1), along with assignments for the nonequivalent protons of each β-methylene group. Chemical shifts for several of these protons were quite similar, as were the chemical shifts of C8^2, C12^2, and C2 (Table 1). HCCH-TOCSY data provided the missing connections between C8^1 and C8^2 and between C12^1 and C12^2 (Figure S10 of the Supporting Information). The slice matching C12^1 exhibited the expected diagonal peaks at 2.8 and 3.0 ppm (Figure 9E). These peaks exhibited cross-peaks to each other and to protons at 2.0 and 2.6 ppm. The mirror resonances from C12^2 were also present in the C2 slice (Figure 9C), completing assignment of the C12-propionate side chain. We were not able to identify a slice corresponding to C8^2. However, a slice corresponding to C8^1 exhibited the expected diagonal peaks at 2.1 and 2.8 ppm (Figure 9G). Each of these peaks exhibited a cross-peak to the other and a cross-peak to a proton at 2.7 ppm, consistent with the values that would be yielded for these atoms by process of elimination from the 12-propionate (Figure S10 of the Supporting Information). The C8^1 slice thus confirmed connections between two independent propionate side chains at C8 and C12, completing assignment of the PCB chromophore of NpR6012g4 in the red-absorbing dark state (Table 1).

Complete Chromophore Assignments for the NpR6012g4 Photoproduct. We employed a similar strategy for complete assignment of the photoproduct state (Figure S5 of the Supporting Information). The one-dimensional ^{13}C spectrum of the photoproduct was again congested (Figure S7D−F of the Supporting Information). The two propionate carbonyl carbons were not resolved from each other (Figure S7D of the Supporting Information), but an aromatic resonance at 125.3 ppm (Figure S7E of the Supporting Information) could be assigned to one or more of C7, C13, or C17 based on data from the partial labeling studies (Figure 2). The aliphatic region exhibited two upfield doublets (Figure S7F of the Supporting Information). The ^{1}H−^{13}C HMQC spectrum was congested (Figure S8B of the Supporting Information), with the photoproduct ct-HSQC spectrum permitting identification of candidate side-chain resonances again including nonequivalent methylene protons (Figure 7B). C6, C8, C12, and C18 remained an unresolved set, as did C7, C13, and C17, and C9 and C11.

The ^{13}C−^{13}C COSY experiment yielded additional information (Figure 10A and Figure S11A−C of the Supporting Information). In addition to expected resonances (e.g., C3−C4), we observed C1−C2, C5−C6, C19−C18, and C18−C18^1 cross-peaks. These resonances permitted assignment of C2, C6, C18, and C18^1 to 36.4, 150.9, 139.3, and 16.6 ppm, respectively (Table 1). Possible additional cross-peaks close to the diagonal implicated assignment of C7 at 127.5 ppm. Three robust cross-peaks connected ring carbons to methyl groups, but peaks linking ring carbons to propionate side chains were much weaker (Figure S11A,B of the Supporting Information). The overlapped propionate γ-carbonyl signals were associated with a complex cross-peak, implicating possible chemical shifts for the γ-carbonyl carbons by reference to the ct-HSQC spectrum (Figure 7B and Figure S11C of the Supporting Information). The C8 and C12 pair and C9 and C11 pair remained to be resolved, as did the set of C7, C13, and C17, and connections between ring carbons and side chains were less complete for the photoproduct than for the dark state.

A carbon-detected ^{13}C−^{13}C TOCSY experiment permitted further progress (Figure 10B). Assignments were again complicated by overlapped resonances, but a different set of overlaps appeared for the photoproduct: one member of the set of C7, C13, and C17 is overlapped with the pair of C9 and C11, whereas another is overlapped with C18. The pair of C8 and C12 had chemical shifts between those of C14 and C16. Working from the known C5 methine bridge confirmed the assignment of C6 and that of C7 at 127.5 ppm, validating a tentative C6−C7 cross-peak in the COSY spectrum (Figure 10A and Figure S11D of the Supporting Information). The remaining pair of C13 and C17 both exhibited cross-peaks to C15, as expected; however, only the well-resolved resonance at 125.3 ppm also exhibited a cross-peak to C14 (Figure S11E of the Supporting Information). This resonance was assigned to C13, implying assignment of C17 to 139.9 ppm. The apparent absence of C17−C18 cross-peaks is thus explained by the similar chemical shift values of these two atoms [139.3 and 139.9 ppm (Table 1)]. C13 also exhibited a cross-peak to one member of the pair of C9 and C11. C6 exhibited cross-peaks to C5, C7, and C8, yielding assignment of C8 as the downfield member of the pair of C8 and C12 (Figure S11F of the Supporting Information). Cross-peaks from C7, C9, and C11 were overlapped (Figure S11G of the Supporting Information), but the C6−C7, C8−C7, C8−C9, and C13−C11 cross-peaks were consistent with C11 as the upfield member of the pair of C9 and C11 and C9 as the downfield member (Table 1). These results thus provided direct assignments for C7−C9, C11, C13, and C17, leading to assignment of C7^1, C13^1, C17^1, and their attached methyl protons by reference to the ct-HSQC and ^{13}C−^{13}C COSY spectra (Table 1).

C13−C12 cross-peaks were absent in ^{13}C−^{13}C COSY and ^{13}C−^{13}C TOCSY spectra, with the only C12 cross-peaks being to C10 and to the overlapped region containing C7, C9, and C11. Given the known photochemical heterogeneity of the NpR6012g4 photoproduct state,[55,57] we could not rule out the possibility that the C12 resonance identified by process of elimination instead represented an alternate chemical shift for C8, which could also give TOCSY cross-peaks to C7, C9, and C10. We therefore performed a ^{13}C−^{13}C NOESY experiment.

DOI: 10.1021/bi501548t
Biochemistry 2015, 54, 2581−2600

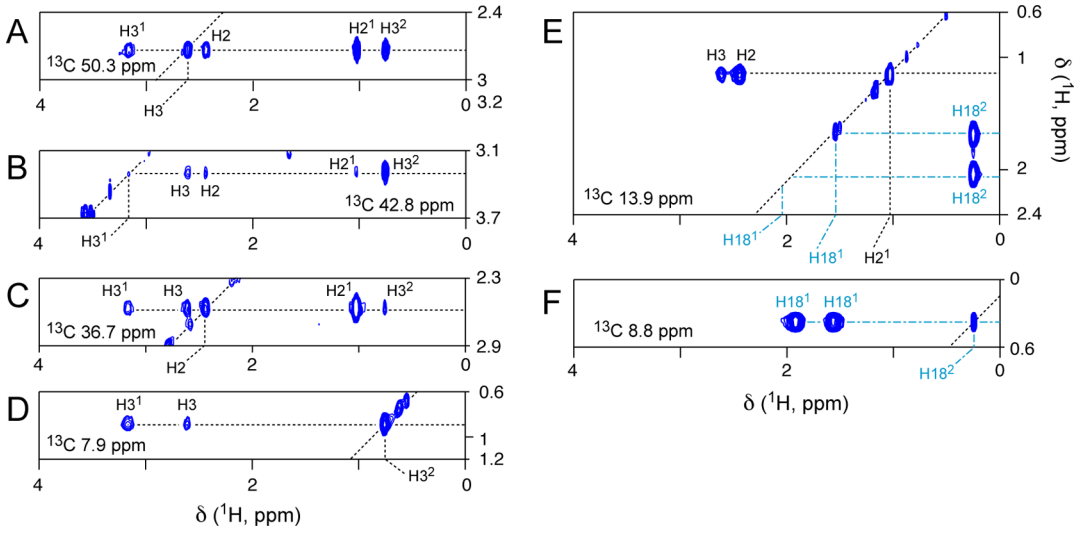

Figure 11. Mapping A-ring and D-ring aliphatic resonances in the green-absorbing NpR6012g4 photoproduct using HCCH-TOCSY. (A–E) Strips matching aliphatic A-ring protons. The slice at 13.9 ppm (E) exhibited strips corresponding to both $C2^1$ and $C18^1$. (F) Reciprocal strip from the $H18^2$ proton. Spectral parameters for HCCH-TOCSY were identical to those of Figure 9.

The resulting carbon-detected NOESY spectrum exhibited a clear C13–C12 cross-peak at the expected location (Figure S11H of the Supporting Information), completing assignment of the ring carbons (Table 1 and Figure S5 of the Supporting Information). Providing an independent validation of this process, cross-peaks previously observed from the set of C6, C8, C12, C14, C16, and C18 in a photoproduct HMBC spectrum on a partially labeled sample partially labeled could now be assigned as three-bond correlations from C6 and C8 to the $H7^1$ methyl protons (Figure S11I of the Supporting Information).

The $^{13}C–^{13}C$ TOCSY spectrum also contained cross-peaks between the tertiary carbons of the A-ring, confirming the tentative assignment for $C3^1$ (Figure 10C) and permitting a walk around the bilin using the carbon-detected COSY, TOCSY, and NOESY spectra. The $^1H–^{13}C$ HMQC spectrum thus permitted tentative assignment of $H3^1$ (Figure S8B of the Supporting Information). We then used a 3D HCCH-TOCSY experiment to complete assignment of the A-ring (Figure 11). Slices matching C2, C3, and $C3^1$ exhibited a consistent pattern of cross-peaks that confirmed the chemical shifts of H2 and $H3^1$ (Figure 11A–C). These slices also provided tentative values for $H3^2$ and $H2^1$ based on the intensity of cross-peaks in the C2 and $C3^1$ slices: a proton at 0.9 ppm exhibited a strong cross-peak to $H3^1$ but a weak cross-peak to H2, whereas a proton at 1.1 ppm instead exhibited a strong cross-peak to H2 but a weak cross-peak to $H3^1$. Assignment of $H2^1$ at 1.1 ppm also was consistent with HMBC cross-peaks from C1 and C3 in the [C4-^{13}C]ALA sample (Figure 4B). The ^{13}C atoms associated with the $H3^2$ and $H2^1$ protons were identified by the ct-HSQC experiment (Figure 7B). HCCH-TOCSY slices matching those carbons confirmed assignment of the $C2^1$ and $C3^2$ methyl groups, because each group exhibited TOCSY cross-peaks to only two neighboring carbons in the expected pattern (Figure 11D,E). The 18-ethyl group was also well-resolved in the HCCH-TOCSY data (Figure 11E,F and Table 1).

Therefore, only the 8- and 12-propionate side chains remained to be assigned for the photoproduct (Figure S5 of the Supporting Information). The HCCH-TOCSY data contained cross-peaks consistent with only one propionate side chain, connecting one α-methylene ($C8^1$ or $C12^1$) to a β-methylene ($C8^2$ or $C12^2$) (Figure 12A,B). We were concerned that the ct-HSQC cross-peaks assigned as a second propionate could instead reflect an alternate propionate conformation. We therefore performed a 3D HCCH-COSY experiment. The expected resonances for the A-ring and D-ring were observed (Figure S12 of the Supporting Information), consistent with assignments obtained by HCCH-TOCSY and ct-HSQC. The propionate detected by HCCH-TOCSY was again detected in the HCCH-COSY spectrum (Figure 12C,D); however, the downfield slice matching the β-methylene also contained signals from a second propionate side chain, matching the ct-HSQC spectrum (Figures 7B and 12D). We were therefore able to identify the mirror slice for the second propionate (Figure 12E). These results thus connected the α-methylene and β-methylene groups of two propionate side chains (Figure S10 of the Supporting Information, green).

Further progress was complicated by the weak $C8–C8^1$ and $C12–C12^1$ cross-peaks observed in the $^{13}C–^{13}C$ COSY spectrum and by the overlapped resonances of the two γ-carbonyl atoms. However, the known chemical shifts of the β-methylene carbons permitted connection of the β-methylene and γ-carbonyl carbons (Figure S11C of the Supporting Information). To connect the known C8 and C12 atoms to the α-methylene carbons, we noted that only four combinations were possible, permitting interpretation of the weak $C8–C8^1$ and $C12–C12^1$ signals and completing assignment of the photoproduct state (Figure S11A,B of the Supporting Information).

Confirmation of the Photoproduct Protonation State Using *ab Initio* Calculations. These assignments were internally consistent, but we did not resolve unambiguous resonances from the B-ring NH moiety in the photoproduct state (see above). This could arise due to deprotonation of the B-ring nitrogen, as predicted by the protochromic model and implied by the solvation model (Figure S2 of the Supporting Information). The fourth HSQC cross-peak would then arise because of an alternate tautomer, for example with a deprotonated C-ring. Deprotonated bilin nitrogen atoms typically exhibit chemical shifts of >200 ppm with low

DOI: 10.1021/bi501548t
Biochemistry 2015, 54, 2581–2600

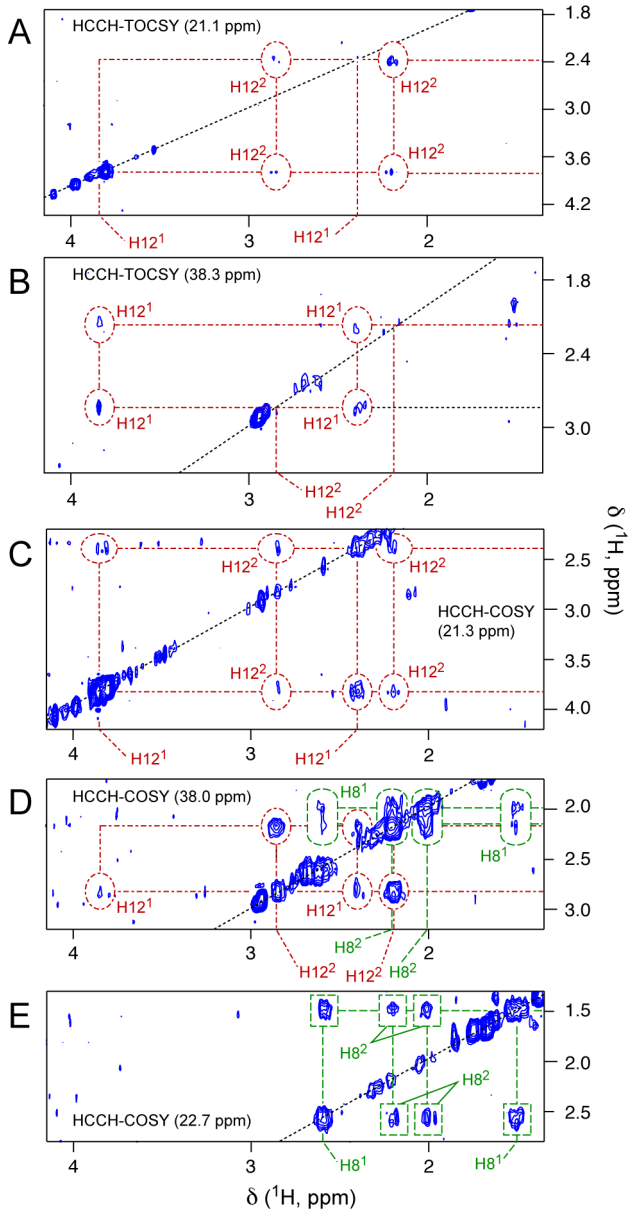

Figure 12. Mapping green-absorbing photoproduct propionate side chains using HCCH-TOCSY and HCCH-COSY. (A–D) Strips matching the 12-propionate were detected in HCCH-TOCSY and HCCH-COSY. (D) The HCCH-COSY slice containing strips from the $H12^2$ protons also exhibited strips from $H8^2$ protons. (E) HCCH-COSY slice containing $H8^1$ strips. Spectral parameters for HCCH-TOCSY were identical to those of Figure 9. For HCCH-COSY, the ^{13}C (F2) and ^1H (F1 and F3) carrier frequencies were 40 and 4.70 ppm, respectively. The three-dimensional acquisition times were 25 ms (F1), 10 ms (F2), and 200 ms (F3).

sensitivity,[77,78] and we were not able to detect ^{15}N directly. However, such deprotonated tautomers formally change both the charge and the electronic structure of the bilin π system, so we reasoned that they would have effects on carbon chemical shifts and on nitrogen chemical shifts. We therefore considered the applicability of *ab initio* deshielding calculations to calculating such changes. We first used a model compound replacing the propionate side chains with methyl groups and lacking the thioether linkage at $C3^1$ (Figure S13A of the Supporting Information). As a test of this approach, we compared B3LYP/6-31G* deshielding values to experimental values previously reported for cyanobacterial phytochrome Cph1 in the 15*Z* P_r state (Figure 13A).[25,27] Agreement was surprisingly good for carbon atoms, validating the approach. Agreement between these calculated values and assignments for dark-state NpR6012g4 was also good (Figure 13A).

We next considered possible photoproduct geometries for NpR6012g4. Chemical denaturation studies have established a 15*E* configuration for the green-absorbing photoproduct state,[39,52,56] but this assay does not provide information about the configuration of the formal 5,6- and 14,15-single bonds. We therefore used TD-DFT calculations to estimate the absorption properties of C15-*E,syn* and C15-*E,anti* geometries of the model compound (Figure S13B,C of the Supporting Information). The C15-*E,anti* configuration gave values in better agreement with experiment (Table 2). Interestingly, this geometry also exhibited a considerable twist of the 14,15-bond (Table S2 of the Supporting Information), making it possible that this geometry mimics a trapped-twist geometry in the actual photoproduct. The twisted 14,15-bond in this model compound arose because of a steric clash between the $C13^1$ and $C17^1$ methyl groups, because it was not seen in a *gedanken* geometry in which those moieties were replaced by hydrogen atoms (Figure S13D and Table S2 of the Supporting Information). This *gedanken* geometry also exhibited a red-shifted vertical excitation energy (Table 2), further implicating a connection between a twisted 14,15-bond and a blue-shifted, green-absorbing 15*E* chromophore.

We therefore selected the C15-*E,anti* configuration as a starting point for testing the effects of bilin protonation on carbon chemical shifts. As a control, deprotonated neutral tautomers in the C15-*Z,anti* configuration exhibited blue shifts relative to the protonated cationic C15-*Z,anti* model compound (Table 2). These blue shifts were also consistent with the known peak absorption of denatured covalent PCB adducts at neutral pH.[51,79] We therefore used the C15-*E,anti* model compound to prepare B- and C-deprotonated tautomers, and all three models were used for B3LYP/6-31G* deshielding and BLYP/6-31G* TD-DFT calculations. Effects of deprotonation on vertical excitation energy in these twisted geometries were surprisingly variable (Table 2): the B-deprotonated neutral tautomer is blue-shifted relative to the protonated model compound (480 nm vs 520 nm), whereas the C-deprotonated neutral tautomer is red-shifted (561 nm). Such an effect was not observed for deprotonated neutral tautomers in the C15-*E,syn* configuration (Table 2). These results suggest that a mix of the two neutral C15-*E,anti* tautomers could give rise to an absorption spectrum having peak absorption similar to that of the protonated photoproduct. If this proves to be true, interpretation of the structure of 15*E* bilins based on absorbance spectroscopy would be complicated by such factors.

However, the same complication did not apply to calculated chemical shift values (Table 3). Importantly, deprotonation at either position produced large changes at C9 and C11 relative to the protonated cationic model compound, along with smaller changes across the ring system. In the B-deprotonated neutral tautomer, C9 is downfield at 139 ppm, with C11 at 119 ppm. The situation is reversed in the C-deprotonated neutral tautomer, with C11 and C9 at 138 and 118 ppm, respectively. By contrast, C9 and C11 have very similar chemical shifts in the protonated cationic model (121 and 119 ppm, respectively) and experimentally [129 and 128.5 ppm, respectively (Table 1)]. The experimental values for C9 and C11 could reflect the presence of two neutral tautomers in fast exchange, such that

DOI: 10.1021/bi501548t
Biochemistry 2015, 54, 2581–2600

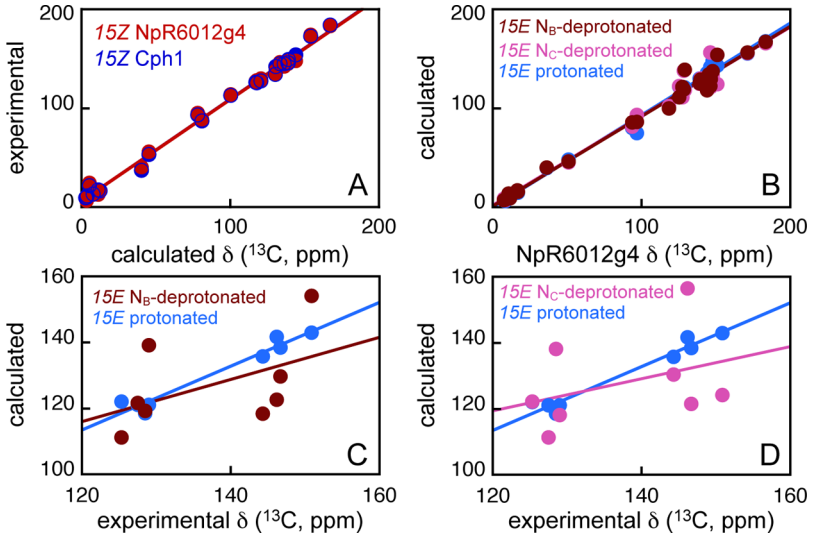

Figure 13. Comparison of experimental and calculated ^{13}C chemical shifts. (A) Calculated chemical shifts for the C15-*Z,anti* configuration (Figure S13A of the Supporting Information) were plotted vs experimentally observed shifts for the bilin chromophores of Cph1 in the P_r state (navy blue, values from ref 27) and NpR6012g4 in the red-absorbing 15*Z* dark state (red, this study). Data were fit by linear regression (Cph1, $r^2 = 0.995$; NpR6012g4, $r^2 = 0.993$; $n = 26$). The nonphysical 8- and 12-side chains and $C3^1$ atom (Figure S13 of the Supporting Information) were omitted from the analysis. (B) Experimentally observed chemical shifts for the NpR6012g4 photoproduct chromophore were fit to calculated chemical shifts for the C15-*E,anti* configuration (Figure S13C of the Supporting Information) with the ring system protonated (blue, $r^2 = 0.99$), with the B-ring nitrogen deprotonated (brick red, $r^2 = 0.98$), and with the C-ring nitrogen deprotonated (dusty rose, $r^2 = 0.98$). (C) Experimental chemical shifts are plotted for aromatic carbons of the B- and C-rings (C6−C9 and C11−C14) vs calculated values for protonated (blue, $r^2 = 0.95$) and B-deprotonated (brick red, $r^2 = 0.24$) model compounds in the C15-*E,anti* configuration. (D) Experimental chemical shifts are plotted for aromatic carbons of the B- and C-rings (C6−C9 and C11−C14) vs calculated values for protonated (blue, $r^2 = 0.95$) and C-deprotonated (dusty rose, $r^2 = 0.13$) model compounds in the C15-*E,anti* configuration.

Table 2. Calculated Absorption Properties for NpR6012g4 Chromophore Models[a]

C15 configuration	13,17-side chains	protonation	E_{vert} (nm)	$\Delta\lambda$ (nm)
Z,anti	methyl	protonated	631	−21
Z,anti	methyl	B-deprotonated	587	−65
Z,anti	methyl	C-deprotonated	596	−56
E,syn	methyl	protonated	627	85
E,syn	methyl	B-deprotonated	576	34
E,syn	methyl	C-deprotonated	602	60
E,anti	methyl	protonated	520	−22
E,anti	methyl	B-deprotonated	480	−62
E,anti	methyl	C-deprotonated	561	19
E,syn	proton	protonated	618	76
E,anti	proton	protonated	589	47

[a]For 15*Z* configurations, TD-DFT calculations were performed as described previously.[73] For 15*E* configurations, TD-DFT calculations were performed on AM1 geometries as described in Materials and Methods. Peak photoproduct absorption of NpR6012g4[52] was used as a reference to calculate $\Delta\lambda$ as observed minus calculated. The known variation of canonical red/green CBCRs in peak photoproduct absorption is 528−556 nm,[52] with the atypical DXCF CBCR NpR5113g1 exhibiting a more blue-shifted photoproduct still after *in vitro* assembly with PCB (516 nm).

we are seeing an average of the two. However, such fast exchange would also produce an averaged value for the two NH moieties, at odds with the four observed resonances in the $^1H-^{15}N$ HSQC spectrum. Moreover, the overall fit of calculated ^{13}C chemical shifts to individually assigned experimental values is markedly superior for the protonated cationic model (Figure 13B), an effect particularly noticeable for carbons in the B- and C-rings (Figure 13C,D). The

Table 3. Calculated ^{13}C Chemical Shifts for the NpR6012g4 Photoproduct[a]

atom	protonated δ	B-deprotonated δ	C-deprotonated δ	observed δ
C1	167.6	167.1	165.7	183.6
C2	39.6	39.8	40.3	36.4
$C2^1$	14.9	15.8	15.9	16.9
C3	48.3	46.4	45.3	51.1
$C3^2$	13.6	13.5	13.4	10.6
C4	147.8	137.5	133.1	148.0
C5	80.2	85.9	81.7	94
C6	142.9	154.1	124.2	150.9
C7	121.0	121.6	111.4	127.5
$C7^1$	6.1	7.9	7.0	8.5
C8	138.5	129.7	121.5	146.7
C9	121	139.1	118.1	129.0
C10	101.3	100.0	102.4	118.5
C11	118.5	119.3	138.1	128.5
C12	135.8	118.4	130.3	144.3
C13	122.1	111.2	122.2	125.3
$C13^1$	6.9	7.3	8.5	7.5
C14	141.7	122.6	156.5	146.2
C15	74.9	86.1	93.2	97.0
C16	137.3	134.5	130.0	145.5
C17	125.5	129.1	129.9	139.9
$C17^1$	9.9	8.9	11.8	11.6
C18	130.2	125.2	124.5	139.3
$C18^1$	17.3	16.9	16.9	16.6
$C18^2$	10.7	11.1	11.1	11.5
C19	155.7	156.2	156.0	171.3

[a]All δ ^{13}C values are reported in parts per million. Deshielding calculations were performed on AM1 geometries as described in Materials and Methods.

DOI: 10.1021/bi501548t
Biochemistry 2015, 54, 2581−2600

deviation between calculated and experimental values for the protonated cationic model (Table 3) is described well by a linear fit (Figure 13B−D), suggesting intrinsic limitations of the gas-phase calculation. By contrast, deviations for deprotonated neutral models have larger, less systematic errors (Figure 13C,D). Thus, both $^{1}H-^{15}N$ and ^{13}C NMR spectroscopy implicate a protonated cationic chromophore π system in the NpR6012g4 photoproduct state.

DISCUSSION

We have obtained complete assignments for all C, H, and N atoms in the PCB chromophore of NpR6012g4 in both photostates. This work sheds new light on bilin structure and protein−chromophore interactions in the abundant red/green CBCR subfamily. Our experiments also extend recently developed carbon-detected NMR techniques from protein backbone assignments to the study of photoprotein chromophores. Despite the known heterogeneity of NpR6012g4,[52,54−57] we detect no heterogeneity in the chromophore itself. It is of course possible that minor populations are present at a level that is too low for detection or are poorly detected due to dynamic exchange. Indeed, the methylene resonances at C18^{1} and in the propionate side chains give rise to much weaker signals in the ct-HSQC spectra than do the side-chain methyl groups. An approximately 3-fold reduction would be expected in this situation, by simple comparison of three equivalent methyl protons to one nonequivalent methylene proton. However, the observed difference was much larger than expected (≥20-fold). The much lower NMR peak heights for the propionate resonances are likely due to exchange broadening, which could arise from conformational flexibility of these side chains. However, conformational exchange of the surrounding protein could also influence peak intensities. Heterogeneity of the surrounding protein matrix could affect the absorption spectrum and quantum yield, as well, so our homogeneous assignments are not inconsistent with heterogeneous primary photochemistry.

Our data provide good evidence of a protonated cationic bilin ring system in both photostates. This conclusion is not surprising for the dark state, because the spectrally and structurally similar red-absorbing state of phytochrome is also protonated.[25,27,49,76,78,80] In the photoproduct state, we were able to observe four bilin NH moieties in HSQC spectra (Figure 6A and Figure S3D of the Supporting Information). HNCO/HNC$_{ar}$ experiments provide unambiguous assignments for three of the four. A process of elimination would imply that the fourth cross-peak corresponds to the protonated NH$_{B}$ moiety, but other interpretations are possible. We therefore compared the observed ^{13}C chemical shifts of the bilin π system to values obtained by *ab initio* calculation. Supporting our interpretation, this comparison does not favor a deprotonated neutral bilin ring system. Therefore, two independent lines of evidence support a protonated cationic bilin ring system in the photoproduct state of NpR6012g4. A protonated photoproduct chromophore population was previously observed in AnPixJg2 by resonance Raman spectroscopy 2.[53] The demonstration of such a photoproduct in NpR6012g4 using solution NMR spectroscopy suggests a conserved mechanism for canonical red/green CBCRs. However, AnPixJg2 and NpR6012g4 are closely related. It will thus be interesting to evaluate other members of this subfamily lacking the conserved "lid Trp" residue[43,52,53] as well as members of the second CBCR subfamily with red/green photocycles, the NpR3784 group.[38]

Our studies do not support the presence of a loosely ordered, extensively solvated photoproduct in NpR6012g4. Were a disordered pocket to allow exposure of the chromophore to bulk solvent, one would expect that the bilin ring system would have a pK_a similar to that under denaturing conditions. Therefore, the known value of this pK_a for denatured NpR6012g4 [5.8 (from ref 51)] would be comparable to the value in such a pocket, implying deprotonation of the bilin π system in such an environment. The presence of a protonated cationic photoproduct in both AnPixJg2[53] and NpR6012g4 (this study) therefore implies the presence of a well-ordered photoproduct structure without bulk solvation. This interpretation is also consistent with characterization of primary photoisomerization of the NpR6012g4 photoproduct using ultrafast pump−probe spectroscopy.[55] On an ultrafast time scale, two subpopulations of the NpR6012g4 photoproduct were inferred because of excitation wavelength dependence of the ground-state bleach and stimulated emission bands. The presence of two subpopulations with such distinct behavior implies discrete structurally distinct photoproduct subpopulations that remain distinct after initial excitation, whereas a solvated pocket should instead behave as a single, broad continuum.

This study does not define a chromophore geometry for either state in NpR6012g4. The 15*Z* dark state is spectrally similar to AnPixJg2 and Cph1, both known to adopt the C5-*Z*,*syn* C10-*Z*,*syn* C15-*Z*,*anti* geometry.[49,80] This spectral similarity implicates a similar chromophore structure in NpR6012g4. An equivalent analogy is not available for the 15*E* photoproduct. TD-DFT calculations on model compounds show that a C15-*E*,*anti* geometry provides better agreement with experiment than a C15-*E*,*syn* geometry (Table 2). The C15-*E*,*anti* geometry also has an intrinsically twisted configuration because of the steric clash between the C13- and C17-methyl moieties in this configuration (Table S2 of the Supporting Information), consistent with the trapped-twist model for photoproduct tuning (Figure 1A).

We also found that deprotonation of the twisted C15-*E*,*anti* geometry to yield neutral bilin π systems does not lead to predictable results in TD-DFT calculations, in contrast to the effect of deprotonation on the more planar C15-*E*,*syn* geometry (Table 2 and Table S2 of the Supporting Information). Deprotonation of the more twisted C15-*E*,*anti* geometry is predicted to yield either a blue shift or a red shift, depending on the deprotonated neutral tautomer. It therefore seems plausible that a mix of the two neutral tautomers could result in a green-absorbing envelope having a peak wavelength similar to that of the protonated, twisted bilin. Presumably, such a case would have a broader photoproduct absorption band because of the two tautomers, but spectral broadening would not be a reliable indicator of chromophore structure. It may prove that red/green CBCR photoproducts will not exhibit conserved protonation states. Such a structural difference could perhaps play a role in tuning other properties of the CBCR, such as quantum yield and/or dark reversion rate.

Our data provide information about structural changes in the NpR6012g4 chromophore-binding pocket upon photoconversion, with changes occurring in C, H, and N atoms. Unlike carbon chemical shifts, hydrogen and nitrogen chemical shifts were not reproduced well by *ab initio* calculations (Figure S14 of the Supporting Information). This is not surprising for bilin NH moieties, which are hydrogen bonded in available phytochrome and CBCR structures[26,48−50,80−86] and hence

DOI: 10.1021/bi501548t
Biochemistry 2015, 54, 2581−2600

are not described well by gas-phase models. We observe good agreement between calculation and experiment for carbon chemical shifts except at C3[1] and at the propionate side chains, which are not accurately described by the model compounds used in calculations (Figure S13 of the Supporting Information) and hence were omitted from fitting. This good overall agreement indicates that chemical shifts for bilin carbon atoms are largely determined by the conjugated system and configuration of the bilin itself rather than by surrounding protein−chromophore interactions. Hydrogen chemical shifts are apparently more sensitive to the surrounding environment, so they must be interpreted with caution. For example, chemical shift changes of ≥0.5 ppm are observed upon photoconversion for H3 and H3[2] in NpR6012g4 (Table 1). Changes of ≥4 ppm are also seen for C2, C2[1], and C3, with a strikingly large change at C3[2]. Such changes could be interpreted as arising due to movement of the A-ring relative to the rest of the chromophore, which is seen in TePixJ.[48−50] However, other interpretations are possible. For example, the A-ring adopts an α-facial disposition in the AnPixJ dark state, but a β-facial disposition in the TePixJ photoproduct.[49] The Cys residue covalently attached to the C3 side chain also rotates, placing the sulfur atom of the thioether in a different position relative to the A-ring. The absence of this sulfur results in poor agreement of calculated and experimental chemical shifts at C3[1], so its movement in the actual protein could produce changes in chemical shifts of A-ring atoms. Such rotation of the thioether linkage could also occur without rotation of the A-ring due to in-plane rotation of the chromophore upon photoconversion (the rotate step of the flip-and-rotate model).[26] Similarly, the downfield change in chemical shift at H10 could arise through changes in its local environment, consistent with a larger downfield shift at H12[1]. We therefore view detailed attempts to interpret the observed chemical shift changes as premature.

Our results do permit comparison between NpR6012g4 and the cyanobacterial phytochrome Cph1, for which complete carbon assignments are also available for the PCB chromophore in both photostates.[25,27] Overall, ^{13}C chemical shifts are very similar for the two proteins in their respective red-absorbing 15*Z* dark states (Figure S15A,B of the Supporting Information). Surprisingly, the ^{13}C chemical shifts for the two photoproduct states are also very similar (Figure S15C,D of the Supporting Information), despite their distinct absorption properties. To compare chemical shift changes upon photoconversion for these two proteins, we calculated $(\delta_{15Z} - \delta_{15E})^2/\delta_{15Z}$ for each C atom in the π system (Figure 14). This unsigned measure was used to focus on the magnitude of change compared to the dark-state chemical shift. Strikingly, changes in Cph1 are largely localized to the vicinity of the C15 methine bridge and the bilin D-ring, whereas the largest changes in the NpR6012g4-conjugated system occur at C5, C10, and C18. It is tempting to interpret changes at C5 and C10 in terms of ring rotation, particularly given the apparent insensitivity of bilin ring carbons to their surrounding environment. However, other interpretations exist. In the trapped-twist model, the D-ring is proposed to be deconjugated to produce the photoproduct blue shift. Such deconjugation would change the bond orders of the rest of the conjugated system, which would be expected to produce changes in chemical shifts. Chromophore movement within the pocket would also produce changes in the sterically favored configurations adopted by the bilin chromophore, for instance

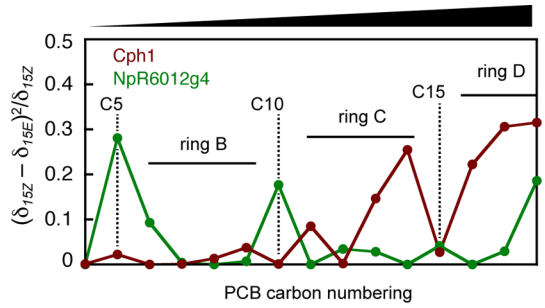

Figure 14. Changes in chemical shift upon photoconversion for NpR6012g4 and Cph1. Changes in chemical shift were calculated as $(\delta_{15Z} - \delta_{15E})^2/\delta_{15Z}$ for NpR6012g4 (green) and Cph1 (brick red).[25,27] Values for the π system are shown, starting with C4 (far left) and ending with C18 (far right). Rings and methine bridges are indicated.

in the allowed values for the dihedral angles of the formal 5,6- and 14,15-single bonds. The observed changes are not consistent with more drastic changes in chromophore structure. For example, formation of a second protein−chromophore linkage produces much greater changes in chemical shift.[63]

Interpretation of the surprising similarity between carbon chemical shifts of the NpR6012g4 and Cph1 photoproducts is not straightforward. The known C15-*E,anti* configuration of the Cph1 P_{fr} state[25] implicates some degree of steric clash between the C13- and C17-methyl groups, as is seen in our gas-phase geometries. It is possible that phytochromes have some means of alleviating this steric clash that is not used by CBCRs, such as an in-plane stretch of the C14−C15−C16 bond angle. Such a motion could effectively extend the length of the conjugated system by stretching the bilin chromophore, leading to the characteristic photoproduct red shift of phytochromes. Were such a motion to be stabilized by structural changes in the conserved "tongue" supplied by the phytochrome PHY domain,[87,88] it would not be seen in CBCRs. In addition to providing new information about chromophore structure in NpR6012g4, our studies thus highlight the importance of protein−chromophore interactions around the photoactive D-ring in producing the far-red-absorbing photoproduct of phytochrome.

■ ASSOCIATED CONTENT

Supporting Information

Fifteen figures and two tables. This material is available free of charge via the Internet at http://pubs.acs.org.

■ AUTHOR INFORMATION

Corresponding Author

*E-mail: jbames@ucdavis.edu.

Funding

This work was supported by a grant from the Chemical Sciences, Geosciences, and Biosciences Division, Office of Basic Energy Sciences, Office of Science, United States Department of Energy (DOE DE-FG02-09ER16117 to J.C.L. and J.B.A.).

Notes

The authors declare no competing financial interest.

■ ACKNOWLEDGMENTS

We thank Jerry L. Dallas and Wolfgang Gärtner for helpful discussions.

DOI: 10.1021/bi501548t
Biochemistry 2015, 54, 2581−2600

■ ABBREVIATIONS

ALA, δ-aminolevulinic acid; CBCR, cyanobacteriochrome; CBD, chitin-binding domain; CCA, complementary chromatic acclimation; COSY, correlation spectroscopy; ct-HSQC, constant-time HSQC; EDTA, ethylenediaminetetraacetic acid; FaRLiP, far-red light photoacclimation; HCCH-COSY, proton−carbon−carbon−proton COSY; HCCH-TOCSY, proton−carbon−carbon−proton TOCSY; HMBC, heteronuclear multiple-bond correlation; HMQC, heteronuclear multiple-quantum coherence; HNCA, proton−nitrogen−Cα; HNC_{ar}, proton−nitrogen−aromatic carbon; HNCO, proton−nitrogen−carbonyl carbon; HSQC, heteronuclear single-quantum coherence; LR-HMQC, long-range HMQC; NMR, nuclear magnetic resonance; NOE, nuclear Overhauser effect; NOESY, NOE spectroscopy; PCB, phycocyanobilin; P_r, red-absorbing 15*Z* dark state of phytochrome; P_{fr}, far-red-absorbing 15*E* photoproduct state of phytochrome; SAR, specific absorbance ratio; TD-DFT, time-dependent density functional theory; TMS, tetramethylsilane; TOCSY, total correlation spectroscopy.

■ REFERENCES

(1) Glazer, A. N. (1985) Light harvesting by phycobilisomes. *Annu. Rev. Biophys. Biophys. Chem. 14*, 47−77.

(2) Frankenberg, N. F., and Lagarias, J. C. (2003) Biosynthesis and biological function of bilins. In *The Porphyrin Handbook. Chlorophylls and Bilins: Biosynthesis Structure and Degradation*. (Kadish, K. M., Smith, K. M., and Guilard, R., Eds.) pp 211−235, Academic Press, New York.

(3) Bibby, T. S., Nield, J., and Barber, J. (2001) Iron deficiency induces the formation of an antenna ring around trimeric photosystem I in cyanobacteria. *Nature 412*, 743−745.

(4) Boekema, E. J., Hifney, A., Yakushevska, A. E., Piotrowski, M., Keegstra, W., Berry, S., Michel, K. P., Pistorius, E. K., and Kruip, J. (2001) A giant chlorophyll-protein complex induced by iron deficiency in cyanobacteria. *Nature 412*, 745−748.

(5) Chen, M., Zhang, Y., and Blankenship, R. E. (2008) Nomenclature for membrane-bound light-harvesting complexes of cyanobacteria. *Photosynth. Res. 95*, 147−154.

(6) Kehoe, D. M., and Gutu, A. (2006) Responding to color: The regulation of complementary chromatic adaptation. *Annu. Rev. Plant Biol. 57*, 127−150.

(7) Gan, F., Zhang, S., Rockwell, N. C., Martin, S. S., Lagarias, J. C., and Bryant, D. A. (2014) Extensive remodeling of a cyanobacterial photosynthetic apparatus in far-red light. *Science 345*, 1312−1317.

(8) Enomoto, G., Nomura, R., Shimada, T., Win, N. N., Narikawa, R., and Ikeuchi, M. (2014) Cyanobacteriochrome SesA is a diguanylate cyclase that induces cell aggregation in *Thermosynechococcus*. *J. Biol. Chem. 289*, 24801−24809.

(9) Yoshihara, S., Suzuki, F., Fujita, H., Geng, X. X., and Ikeuchi, M. (2000) Novel putative photoreceptor and regulatory genes required for the positive phototactic movement of the unicellular motile cyanobacterium *Synechocystis* sp. PCC 6803. *Plant Cell Physiol. 41*, 1299−1304.

(10) Bhaya, D., Takahashi, A., and Grossman, A. R. (2001) Light regulation of type IV pilus-dependent motility by chemosensor-like elements in *Synechocystis* PCC6803. *Proc. Natl. Acad. Sci. U.S.A. 98*, 7540−7545.

(11) Bhaya, D. (2004) Light matters: Phototaxis and signal transduction in unicellular cyanobacteria. *Mol. Microbiol. 53*, 745−754.

(12) Yoshihara, S., Katayama, M., Geng, X., and Ikeuchi, M. (2004) Cyanobacterial Phytochrome-like PixJ1 Holoprotein Shows Novel Reversible Photoconversion Between Blue- and Green-absorbing Forms. *Plant Cell Physiol. 45*, 1729−1737.

(13) Narikawa, R., Suzuki, F., Yoshihara, S., Higashi, S. I., Watanabe, M., and Ikeuchi, M. (2011) Novel Photosensory Two-Component System (PixA-NixB-NixC) Involved in the Regulation of Positive and Negative Phototaxis of Cyanobacterium *Synechocystis* sp. PCC 6803. *Plant Cell Physiol. 52*, 2214−2224.

(14) Song, J. Y., Cho, H. S., Cho, J. I., Jeon, J. S., Lagarias, J. C., and Park, Y. I. (2011) Near-UV cyanobacteriochrome signaling system elicits negative phototaxis in the cyanobacterium *Synechocystis* sp. PCC 6803. *Proc. Natl. Acad. Sci. U.S.A. 108*, 10780−10785.

(15) Savakis, P., De Causmaecker, S., Angerer, V., Ruppert, U., Anders, K., Essen, L. O., and Wilde, A. (2012) Light-induced alteration of c-di-GMP level controls motility of *Synechocystis* sp. PCC 6803. *Mol. Microbiol. 85*, 239−251.

(16) Campbell, E. L., Hagen, K. D., Chen, R., Risser, D. D., Ferreira, D. P., and Meeks, J. C. (2015) Genetic analysis reveals the identity of the photoreceptor for phototaxis in hormogonium filaments of *Nostoc punctiforme*. *J. Bacteriol. 197*, 782−791.

(17) Kehoe, D. M., and Grossman, A. R. (1996) Similarity of a Chromatic Adaptation Sensor to Phytochrome and Ethylene Receptors. *Science 273*, 1409−1412.

(18) Yeh, K.-C., Wu, S.-H., Murphy, J. T., and Lagarias, J. C. (1997) A cyanobacterial phytochrome two-component light sensory system. *Science 277*, 1505−1508.

(19) Hirose, Y., Shimada, T., Narikawa, R., Katayama, M., and Ikeuchi, M. (2008) Cyanobacteriochrome CcaS is the green light receptor that induces the expression of phycobilisome linker protein. *Proc. Natl. Acad. Sci. U.S.A. 105*, 9528−9533.

(20) Hirose, Y., Narikawa, R., Katayama, M., and Ikeuchi, M. (2010) Cyanobacteriochrome CcaS regulates phycoerythrin accumulation in *Nostoc punctiforme*, a group II chromatic adapter. *Proc. Natl. Acad. Sci. U.S.A. 107*, 8854−8859.

(21) Lagarias, J. C., and Rapoport, H. (1980) Chromopeptides from phytochrome. The structure and linkage of the Pr form of the phytochrome chromophore. *J. Am. Chem. Soc. 102*, 4821−4828.

(22) Hughes, J. (2010) Phytochrome three-dimensional structures and functions. *Biochem. Soc. Trans. 38*, 710−716.

(23) Rockwell, N. C., and Lagarias, J. C. (2010) A brief history of phytochromes. *ChemPhysChem 11*, 1172−1180.

(24) Auldridge, M. E., and Forest, K. T. (2011) Bacterial phytochromes: More than meets the light. *Crit. Rev. Biochem. Mol. Biol. 46*, 67−88.

(25) Song, C., Psakis, G., Lang, C., Mailliet, J., Gartner, W., Hughes, J., and Matysik, J. (2011) Two ground state isoforms and a chromophore D-ring photoflip triggering extensive intramolecular changes in a canonical phytochrome. *Proc. Natl. Acad. Sci. U.S.A. 108*, 3842−3847.

(26) Yang, X., Ren, Z., Kuk, J., and Moffat, K. (2011) Temperature-scan cryocrystallography reveals reaction intermediates in bacteriophytochrome. *Nature 479*, 428−432.

(27) Song, C., Psakis, G., Kopycki, J., Lang, C., Matysik, J., and Hughes, J. (2014) The D-ring, Not the A-ring, Rotates in *Synechococcus* OS-B′ Phytochrome. *J. Biol. Chem. 289*, 2552−2562.

(28) Butler, W. L., Norris, K. H., Seigelman, H. W., and Hendricks, S. B. (1959) Detection, assay, and preliminary purification of the pigment controlling photoresponsive development of plants. *Proc. Natl. Acad. Sci. U.S.A. 45*, 1703−1708.

(29) Kidd, D. G., and Lagarias, J. C. (1990) Phytochrome from the green alga *Mesotaenium caldariorum*. Purification and preliminary characterization. *J. Biol. Chem. 265*, 7029−7035.

(30) Davis, S. J., Vener, A. V., and Vierstra, R. D. (1999) Bacteriophytochromes: Phytochrome-like photoreceptors from non-photosynthetic eubacteria. *Science 286*, 2517−2520.

(31) Giraud, E., Fardoux, J., Fourier, N., Hannibal, L., Genty, B., Bouyer, P., Dreyfus, B., and Vermeglio, A. (2002) Bacteriophytochrome controls photosystem synthesis in anoxygenic bacteria. *Nature 417*, 202−205.

(32) Froehlich, A. C., Noh, B., Vierstra, R. D., Loros, J., and Dunlap, J. C. (2005) Genetic and molecular analysis of phytochromes from the filamentous fungus *Neurospora crassa*. *Eukaryotic Cell 4*, 2140−2152.

DOI: 10.1021/bi501548t
Biochemistry 2015, 54, 2581−2600

(33) Brandt, S., von Stetten, D., Gunther, M., Hildebrandt, P., and Frankenberg-Dinkel, N. (2008) The fungal phytochrome FphA from *Aspergillus nidulans*. *J. Biol. Chem. 283*, 34605−34614.
(34) De Riso, V., Raniello, R., Maumus, F., Rogato, A., Bowler, C., and Falciatore, A. (2009) Gene silencing in the marine diatom *Phaeodactylum tricornutum*. *Nucleic Acids Res. 37*, e96.
(35) Duanmu, D., Bachy, C., Sudek, S., Wong, C. H., Jimenez, V., Rockwell, N. C., Martin, S. S., Ngan, C. Y., Reistetter, E. N., van Baren, M. J., Price, D. C., Wei, C. L., Reyes-Prieto, A., Lagarias, J. C., and Worden, A. Z. (2014) Marine algae and land plants share conserved phytochrome signaling systems. *Proc. Natl. Acad. Sci. U.S.A. 111*, 15827−15832.
(36) Rockwell, N. C., Duanmu, D., Martin, S. S., Bachy, C., Price, D. C., Bhattacharya, D., Worden, A. Z., and Lagarias, J. C. (2014) Eukaryotic algal phytochromes span the visible spectrum. *Proc. Natl. Acad. Sci. U.S.A. 111*, 3871−3876.
(37) Ikeuchi, M., and Ishizuka, T. (2008) Cyanobacteriochromes: A new superfamily of tetrapyrrole-binding photoreceptors in cyanobacteria. *Photochem. Photobiol. Sci. 7*, 1159−1167.
(38) Rockwell, N. C., Martin, S. S., Gan, F., Bryant, D. A., and Lagarias, J. C. (2015) NpR3784 is the prototype for a distinctive group of red/green cyanobacteriochromes using alternative Phe residues for photoproduct tuning. *Photochem. Photobiol. Sci. 14*, 258−269.
(39) Narikawa, R., Fukushima, Y., Ishizuka, T., Itoh, S., and Ikeuchi, M. (2008) A novel photoactive GAF domain of cyanobacteriochrome AnPixJ that shows reversible green/red photoconversion. *J. Mol. Biol. 380*, 844−855.
(40) Rockwell, N. C., Njuguna, S. L., Roberts, L., Castillo, E., Parson, V. L., Dwojak, S., Lagarias, J. C., and Spiller, S. C. (2008) A second conserved GAF domain cysteine is required for the blue/green photoreversibility of cyanobacteriochrome Tlr0924 from *Thermosynechococcus elongatus*. *Biochemistry 47*, 7304−7316.
(41) Rockwell, N. C., Martin, S. S., Feoktistova, K., and Lagarias, J. C. (2011) Diverse two-cysteine photocycles in phytochromes and cyanobacteriochromes. *Proc. Natl. Acad. Sci. U.S.A. 108*, 11854−11859.
(42) Narikawa, R., Enomoto, G., Ni, W., Fushimi, K., and Ikeuchi, M. (2014) A New Type of Dual-Cys Cyanobacteriochrome GAF Domain Found in Cyanobacterium *Acaryochloris marina*, Which Has an Unusual Red/Blue Reversible Photoconversion Cycle. *Biochemistry 53*, 5051−5059.
(43) Rockwell, N. C., Martin, S. S., Gulevich, A. G., and Lagarias, J. C. (2014) Conserved phenylalanine residues are required for blue-shifting of cyanobacteriochrome photoproducts. *Biochemistry 53*, 3118−3130.
(44) Enomoto, G., Hirose, Y., Narikawa, R., and Ikeuchi, M. (2012) Thiol-based photocycle of the blue and teal light-sensing cyanobacteriochrome Tlr1999. *Biochemistry 51*, 3050−3058.
(45) Rockwell, N. C., Martin, S. S., Gulevich, A. G., and Lagarias, J. C. (2012) Phycoviolobilin formation and spectral tuning in the DXCF cyanobacteriochrome subfamily. *Biochemistry 51*, 1449−1463.
(46) Ishizuka, T., Kamiya, A., Suzuki, H., Narikawa, R., Noguchi, T., Kohchi, T., Inomata, K., and Ikeuchi, M. (2011) The cyanobacteriochrome, TePixJ, isomerizes its own chromophore by converting phycocyanobilin to phycoviolobilin. *Biochemistry 50*, 953−961.
(47) Rockwell, N. C., Martin, S. S., and Lagarias, J. C. (2012) Mechanistic Insight into the Photosensory Versatility of DXCF Cyanobacteriochromes. *Biochemistry 51*, 3576−3585.
(48) Burgie, E. S., Walker, J. M., Phillips, G. N., Jr., and Vierstra, R. D. (2013) A photo-labile thioether linkage to phycoviolobilin provides the foundation for the blue/green photocycles in DXCF-cyanobacteriochromes. *Structure 21*, 88−97.
(49) Narikawa, R., Ishizuka, T., Muraki, N., Shiba, T., Kurisu, G., and Ikeuchi, M. (2013) Structures of cyanobacteriochromes from phototaxis regulators AnPixJ and TePixJ reveal general and specific photoconversion mechanism. *Proc. Natl. Acad. Sci. U.S.A. 110*, 918−923.
(50) Cornilescu, C. C., Cornilescu, G., Burgie, E. S., Markley, J. L., Ulijasz, A. T., and Vierstra, R. D. (2014) Dynamic structural changes underpin photoconversion of a blue/green cyanobacteriochrome between its dark and photoactivated states. *J. Biol. Chem. 289*, 3055−3065.
(51) Hirose, Y., Rockwell, N. C., Nishiyama, K., Narikawa, R., Ukaji, Y., Inomata, K., Lagarias, J. C., and Ikeuchi, M. (2013) Green/red cyanobacteriochromes regulate complementary chromatic acclimation via a protochromic photocycle. *Proc. Natl. Acad. Sci. U.S.A. 110*, 4974−4979.
(52) Rockwell, N. C., Martin, S. S., and Lagarias, J. C. (2012) Red/Green Cyanobacteriochromes: Sensors of Color and Power. *Biochemistry 51*, 9667−9677.
(53) Velazquez Escobar, F., Utesch, T., Narikawa, R., Ikeuchi, M., Mroginski, M. A., Gartner, W., and Hildebrandt, P. (2013) Photoconversion Mechanism of the Second GAF Domain of Cyanobacteriochrome AnPixJ and the Cofactor Structure of Its Green-Absorbing State. *Biochemistry 52*, 4871−4880.
(54) Kim, P. W., Freer, L. H., Rockwell, N. C., Martin, S. S., Lagarias, J. C., and Larsen, D. S. (2012) Second-Chance Initiation Dynamics of the Cyanobacterial Photocycle in the NpR6012 GAF4 Domain of *Nostoc punctiforme*. *J. Am. Chem. Soc. 134*, 130−133.
(55) Kim, P. W., Freer, L. H., Rockwell, N. C., Martin, S. S., Lagarias, J. C., and Larsen, D. S. (2012) Femtosecond Photodynamics of the Red/Green Cyanobacteriochrome NpR6012g4 from *Nostoc punctiforme*. 2. Reverse Dynamics. *Biochemistry 51*, 619−630.
(56) Kim, P. W., Freer, L. H., Rockwell, N. C., Martin, S. S., Lagarias, J. C., and Larsen, D. S. (2012) Femtosecond Photodynamics of the Red/Green Cyanobacteriochrome NpR6012g4 from *Nostoc punctiforme*. 1. Forward Dynamics. *Biochemistry 51*, 608−618.
(57) Chang, C. W., Gottlieb, S. M., Kim, P. W., Rockwell, N. C., Lagarias, J. C., and Larsen, D. S. (2013) Reactive ground-state pathways are not ubiquitous in red/green cyanobacteriochromes. *J. Phys. Chem. B 117*, 11229−11238.
(58) Gottlieb, S. M., Kim, P. W., Chang, C. W., Hanke, S. J., Hayer, R. J., Rockwell, N. C., Martin, S. S., Lagarias, J. C., and Larsen, D. S. (2015) Conservation and diversity in the primary forward photodynamics of red/green cyanobacteriochromes. *Biochemistry 54*, 1028−1042.
(59) Schmidt, M., Patel, A., Zhao, Y., and Reuter, W. (2007) Structural basis for the photochemistry of α-phycoerythrocyanin. *Biochemistry 46*, 416−423.
(60) Fukushima, Y., Iwaki, M., Narikawa, R., Ikeuchi, M., Tomita, Y., and Itoh, S. (2011) Photoconversion mechanism of a green/red photosensory cyanobacteriochrome AnPixJ: Time-resolved optical spectroscopy and FTIR analysis of the AnPixJ-GAF2 domain. *Biochemistry 50*, 6328−6339.
(61) Xu, X. L., Gutt, A., Mechelke, J., Raffelberg, S., Tang, K., Miao, D., Valle, L., Borsarelli, C. D., Zhao, K. H., and Gartner, W. (2014) Combined mutagenesis and kinetics characterization of the bilin-binding GAF domain of the protein Slr1393 from the Cyanobacterium *Synechocystis* PCC6803. *ChemBioChem 15*, 1190−1199.
(62) Narikawa, R., Nakajima, T., Aono, Y., Fushimi, K., Enomoto, G., Ni, W., Itoh, S., Sato, M., and Ikeuchi, M. (2015) A biliverdin-binding cyanobacteriochrome from the chlorophyll d-bearing cyanobacterium *Acaryochloris marina*. *Sci. Rep. 5*, 7950.
(63) Lim, S., Rockwell, N. C., Martin, S. S., Dallas, J. L., Lagarias, J. C., and Ames, J. B. (2014) Photoconversion changes bilin chromophore conjugation and protein secondary structure in the violet/orange cyanobacteriochrome NpF2163g3. *Photochem. Photobiol. Sci. 13*, 951−962.
(64) Lim, S., Rockwell, N. C., Martin, S. S., Lagarias, J. C., and Ames, J. B. (2014) ^{1}H, ^{15}N, and ^{13}C chemical shift assignments of cyanobacteriochrome NpF2164g3 in the photoproduct state. *Biomol. NMR Assignments 8*, 259−262.
(65) Delaglio, F., Grzesiek, S., Vuister, G. W., Zhu, G., Pfeifer, J., and Bax, A. (1995) NMRPipe: A multidimensional spectral processing system based on UNIX pipes. *J. Biomol. NMR 6*, 277−293.
(66) Piotto, M., Saudek, V., and Sklenar, V. (1992) Gradient-tailored excitation for single-quantum NMR spectroscopy of aqueous solutions. *J. Biomol. NMR 2*, 661−665.

DOI: 10.1021/bi501548t
Biochemistry 2015, 54, 2581−2600

(67) Kay, L. E., Ikura, M., Tschudin, R., and Bax, A. (1990) Three-dimensional triple-resonance NMR spectroscopy of isotopically enriched proteins. *J. Magn. Reson. 89*, 496−514.
(68) Bax, A., and Subramanian, S. (1986) Sensitivity-Enhanced Two-Dimensional Heteronuclear Shift Correlation NMR Spectroscopy. *J. Magn. Reson. 67*, 565−569.
(69) Bax, A., and Marion, D. (1988) Improved resolution and sensitivity in H-1 detected heteronuclear multiple bond correlation spectroscopy. *J. Magn. Reson. 78*, 186−191.
(70) Bode, B. M., and Gordon, M. S. (1998) MacMolPlt: A graphical user interface for GAMESS. *J. Mol. Graphics Modell. 16*, 133−138.
(71) Schmidt, M. W., Baldridge, K. K., Boatz, J. A., Elbert, S. T., Gordon, M. S., Jensen, J. H., Koseki, S., Matsunaga, N., Nguyen, K. A., Su, S., Windus, T. L., Dupuis, M., and Montgomery, J. A., Jr. (1993) General atomic and molecular electronic structure system. *J. Comput. Chem. 14*, 1347−1363.
(72) Frisch, M. J., Trucks, G. W., Schlegel, H. B., Scuseria, G. E., Robb, M. A., Cheeseman, J. R., Montgomery, J. A., Jr., Vreven, T., Kudin, K. N., Burant, J. C., Millam, J. M., Iyengar, S. S., Tomasi, J., Barone, V., Mennucci, B., Cossi, M., Scalmani, G., Rega, N., Petersson, G. A., Nakatsuji, H., Hada, M., Ehara, M., Toyota, K., Fukuda, R., Hasegawa, J., Ishida, M., Nakajima, T., Honda, Y., Kitao, O., Nakai, H., Klene, M., Li, X., Knox, J. E., Hratchian, H. P., Cross, J. B., Bakken, V., Adamo, C., Jaramillo, J., Gomperts, R., Stratmann, R. E., Yazyev, O., Austin, A. J., Cammi, R., Pomelli, C., Ochterski, J. W., Ayala, P. Y., Morokuma, K., Voth, G. A., Salvador, P., Dannenberg, J. J., Zakrzewski, V. G., Dapprich, S., Daniels, A. D., Strain, M. C., Farkas, O., Malick, D. K., Rabuck, A. D., Raghavachari, K., Foresman, J. B., Ortiz, J. V., Cui, Q., Baboul, A. G., Clifford, S., Cioslowski, J., Stefanov, B. B., Liu, G., Liashenko, A., Piskorz, P., Komaromi, I., Martin, R. L., Fox, D. J., Keith, T., Al-Laham, M. A., Peng, C. Y., Nanayakkara, A., Challacombe, M., Gill, P. M. W., Johnson, B., Chen, W., Wong, M. W., Gonzalez, C., and Pople, J. A. (2004) *Gaussian03*, revision D.01, Gaussian, Inc., Wallingford, CT.
(73) Rockwell, N. C., Shang, L., Martin, S. S., and Lagarias, J. C. (2009) Distinct classes of red/far-red photochemistry within the phytochrome superfamily. *Proc. Natl. Acad. Sci. U.S.A. 106*, 6123−6127.
(74) van Thor, J. J., Mackeen, M., Kuprov, I., Dwek, R. A., and Wormald, M. R. (2006) Chromophore structure in the photocycle of the cyanobacterial phytochrome Cph1. *Biophys. J. 91*, 1811−1822.
(75) Rodriguez-Mias, R. A., and Pellecchia, M. (2003) Use of selective Trp side chain labeling to characterize protein-protein and protein-ligand interactions by NMR spectroscopy. *J. Am. Chem. Soc. 125*, 2892−2893.
(76) Strauss, H. M., Hughes, J., and Schmieder, P. (2005) Heteronuclear solution-state NMR studies of the chromophore in cyanobacterial phytochrome Cph1. *Biochemistry 44*, 8244−8250.
(77) Falk, H. (1989) *The Chemistry of Linear Oligopyrroles and Bile Pigments*, Springer-Verlag, Vienna.
(78) Hahn, J., Kuhne, R., and Schmieder, P. (2007) Solution-state ^{15}N NMR spectroscopic study of α-C-phycocyanin: Implications for the structure of the chromophore-binding pocket of the cyanobacterial phytochrome Cph1. *ChemBioChem 8*, 2249−2255.
(79) Shang, L., Rockwell, N. C., Martin, S. S., and Lagarias, J. C. (2010) Biliverdin amides reveal roles for propionate side chains in bilin reductase recognition and in holophytochrome assembly and photoconversion. *Biochemistry 49*, 6070−6082.
(80) Essen, L. O., Mailliet, J., and Hughes, J. (2008) The structure of a complete phytochrome sensory module in the Pr ground state. *Proc. Natl. Acad. Sci. U.S.A. 105*, 14709−14714.
(81) Wagner, J. R., Brunzelle, J. S., Forest, K. T., and Vierstra, R. D. (2005) A light-sensing knot revealed by the structure of the chromophore binding domain of phytochrome. *Nature 438*, 325−331.
(82) Wagner, J. R., Zhang, J., Brunzelle, J. S., Vierstra, R. D., and Forest, K. T. (2007) High resolution structure of *Deinococcus* bacteriophytochrome yields new insights into phytochrome architecture and evolution. *J. Biol. Chem. 282*, 12298−12309.
(83) Yang, X., Stojkovic, E. A., Kuk, J., and Moffat, K. (2007) Crystal structure of the chromophore binding domain of an unusual bacteriophytochrome, RpBphP3, reveals residues that modulate photoconversion. *Proc. Natl. Acad. Sci. U.S.A. 104*, 12571−12576.
(84) Yang, X., Kuk, J., and Moffat, K. (2008) Crystal structure of *Pseudomonas aeruginosa* bacteriophytochrome: Photoconversion and signal transduction. *Proc. Natl. Acad. Sci. U.S.A. 105*, 14715−14720.
(85) Yang, X., Kuk, J., and Moffat, K. (2009) Conformational differences between the Pfr and Pr states in *Pseudomonas aeruginosa* bacteriophytochrome. *Proc. Natl. Acad. Sci. U.S.A. 106*, 15639−15644.
(86) Bellini, D., and Papiz, M. Z. (2012) Structure of a bacteriophytochrome and light-stimulated protomer swapping with a gene repressor. *Structure 20*, 1436−1446.
(87) Stojkovic, E. A., Toh, K. C., Alexandre, M. T., Baclayon, M., Moffat, K., and Kennis, J. T. (2014) FTIR Spectroscopy Revealing Light-Dependent Refolding of the Conserved Tongue Region of Bacteriophytochrome. *J. Phys. Chem. Lett. 5*, 2512−2515.
(88) Takala, H., Bjorling, A., Berntsson, O., Lehtivuori, H., Niebling, S., Hoernke, M., Kosheleva, I., Henning, R., Menzel, A., Ihalainen, J. A., and Westenhoff, S. (2014) Signal amplification and transduction in phytochrome photosensors. *Nature 509*, 245−248.

DOI: 10.1021/bi501548t
Biochemistry 2015, 54, 2581−2600